

A novel framework for medium-term wind power prediction based on temporal attention mechanisms

Meiyu Jiang¹, Xuetao Jiang¹, Rui Zhou¹, and Qingguo Zhou^{*2}

¹*School of Information Science and Engineering, Lanzhou University, Lanzhou, 730000, China.
Email: jiangmy21@lzu.edu.cn Email: jiangxt21@lzu.edu.cn Email: zr@lzu.edu.cn*

²*School of Information Science and Engineering, Lanzhou University, Lanzhou, 730000, China.
Email: zhouqg@lzu.edu.cn*

1 Introduction

Energy is essential for economic and global energy demand grows rapidly with the development of the economy and technology. Traditional energy sources such as coal, crude oil and natural gas are burned to generate electricity and emit more than 75% of the world's greenhouse gases, with approximately 90% of the world's carbon dioxide emissions [1]. This is the leading cause of global climate change. Traditional energy sources have limited reserves and can be depleted if overexploited [2]. Due to the non-renewable nature of traditional energy sources, the issue of present energy industry is revealed, and the prices of traditional energy sources are maintained at high levels and are gradually increasing. In order to handle the energy crisis, more and more countries choose the renewable energy as an alternative energy sources. Renewable energy includes wind, solar, tidal and biomass energy, which has the advantages of being widely distributed, recyclable and environment friendly. With the rapid development of wind power technology, converting wind energy into electricity is becoming more efficient and less costly. Wind power plays an essential role in the growth of global electricity generation and has received widespread attention worldwide.

According to the Global Wind Report 2022 [3], the total installed capacity of wind power installations worldwide will be 837 GW in 2021, an increase of 12% compared to 2020. Newly installed wind installations increased by 93.6 GW, slightly more than the 93 GW increase in 2020. China has led the global wind energy industry since 2010, with newly installed wind power capacity increasing significantly over the last 11 years and remaining at the top of the world. According to the National Energy Administration (NEA), the total installed capacity of wind power in China is 52GW in 2021, with 47.5GW of new grid-connected capacity.

The principle of wind power is that wind energy is first converted into mechanical energy and then into electrical energy. Wind energy is characterized by high uncertainty, discontinuity and frequent fluctuations. So, wind turbine power generation is unstable and difficult to predict, affecting the scheduling and planning of power systems and leading to power supply and demand imbalances. To solve these problems, we need to make accurate forecasts of future wind power generation, which helps to reduce costs and increase power generation efficiency. Wind power technology is therefore becoming increasingly important in the field of renewable energy.

Wind power forecasting models can be classified as ultra-short-term, short-term, medium-term and long-term depending on the time horizon [4, 5, 6, 7], as shown in Figure 1. The division of time scales differs from literature to literature, and there are differences in the specific wind power generation applications. The ultra-short-term forecasting model facilitates real-time access to wind power generation. Short-term forecasting models are helpful for power companies to develop load dispatching plans, mitigate the impact of wind power grid integration on the entire grid and ensure the safe operation of the electricity market. Medium-term forecasting models facilitate renewable

arXiv:2302.01222v3 [cs.LG] 28 Apr 2023

Pre-printed in Arxiv (2023)

DOI: 10.1017/pan.xxxx.xx

Corresponding author
Qingguo Zhou

© The Author(s) 2023. Published for Arxiv pre-print.

energy trading, optimization of generation schedules, and circuit overhauls. Long-term forecasting models employ maintenance planning, the location of wind farms, and the development of annual generation plans. Some literature suggests that the accuracy of predictions decreases as the time horizon increases [8, 5, 9]. Also, given the high instability of the wind, it is more difficult to predict if the time horizon chosen is too long. Therefore, this paper focuses on medium-term wind power forecasting.

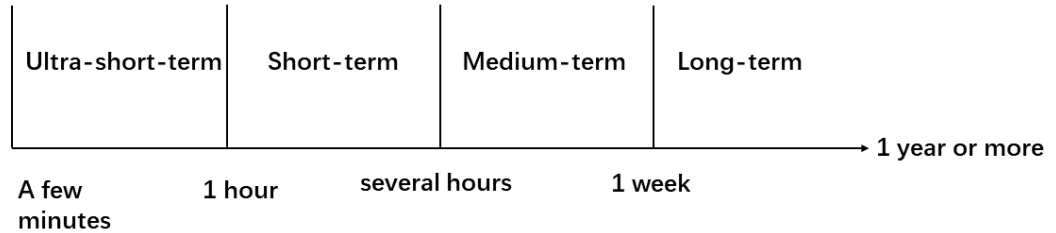


Figure 1. Time-scale classification of wind power forecasting.

2 Literature review

According to modeling theory, wind power models can be classified into four groups: physical models, traditional statistical models, artificial intelligence-based models and hybrid models [10].

The physical approach does not require historical wind power generation data, but relies on the physical characteristics of the wind farm. Physical models can obtain predicted wind power generation values by predicting meteorological variables [11]. The meteorological variables here usually refer to wind speeds, which can be derived from numerical weather prediction (NWP) or from the meteorological factors such as temperature, humidity and atmospheric pressure. The conversion of wind speed and wind power can be obtained from wind power curves. The wind power curve is a graph that shows the power of a wind turbine at different wind speeds, created by researchers measuring wind speeds at wind farms. Furthermore, showing the wind turbine's power output at different wind speeds. Ackermann et al. [12] show that the wind turbine power is proportional to the third power of the wind speed in wind power curves. If there is a 10% error in the predicted wind speed, the error in the predicted wind turbine power will be 30%. Therefore, accurate prediction of wind speed is important for wind power forecasting. There are many papers that use physical model-based solutions for wind power forecasting. For example, Lazić et al. [13] use the regional NWP Eta model for wind farms to obtain predicted wind speed and then predict wind power based on the wind power curve. This paper is the first to evaluate the application of the Eta model to wind power prediction problems and to validate it using data from the Gotland island power plant. The results show that the Eta model can be used as a meteorological driver for wind power prediction. Focken et al. [14] propose a wind power prediction system based on the physical approach with inputs from a large German weather prediction model. The physical approach performs better in long-term wind power forecasting, while the statistical approach has advantages in short-term forecasting [15].

Statistical models require large amounts of data, such as historical power values of wind turbines, historical weather data and weather information to train a fitted model between input and output power. Statistical models can be classified into two types depending on used parameters: parametric models like time series models, and non-parametric models based on artificial intelligence such as artificial neural network (ANN) models and other data-driven models.

Time series models are advantageous for short-term or ultra-short-term wind power forecasting, which could capture fluctuating variations in output power. Autoregressive integrated moving average (ARIMA) and autoregressive (AR) model are commonly used univariate time series forecast-

ing methods. They have a short computation time and are suitable for smooth time series, which can lead to inaccurate predictions with volatile input data. Many methods based on traditional statistical models have been proposed to improve the accuracy of wind speed predictions, and then use the wind power curve to convert wind speed to wind power. Yatiyana et al. [16] propose a statistical method for predicting wind speed and direction based on an ARIMA model. They use data from a specific site in western Australia for validation, with a time duration of 7 days and a resolution of one minute. The experimental results show that the error in predicting wind speed is less than 5%, and the error in predicting wind direction is less than 16%. Firat et al. [17] propose a statistical method for wind speed prediction based on second order blind identification (SOBI) and AR model. SOBI is an ICA method that uses temporal structure to find hidden information or independent components in the input data, providing better prediction results than the direct wind speed prediction.

Physical models require more detailed meteorological data and physical characteristics, which are more demanding on the data set. Moreover, wind turbines are complex and the wind-to-electricity conversion pattern is difficult to model. Traditional statistical models deal mainly with linear relationships, making it difficult to capture the characteristics between non-linear time-series wind power signal sequences. With the development of artificial intelligence techniques, many ANN-based methods have been proposed in the literature on wind power forecasting. Bilal et al. [18] proposed an ANN-based model for predicting wind turbine power. The input features are meteorological factors such as wind speed, wind direction, solar irradiance, temperature and humidity. The experimental results show that using meteorological factors as inputs to the ANN impacts the model's performance, with the most significant impact when wind direction and wind speed were used as feature inputs, and the accuracy of the prediction results was significantly improved. Xu et al. [19] used an Elman neural network to predict short-term wind power generation, which has input features from the NWP and the optimization algorithm using particle swarm optimization (PSO), which can improve the accuracy of the prediction and avoid the problem that the neural network only achieves a local optimum. Jyothi et al. [20] used adaptive wavelet neural network (AWNN) for wind power generation. In addition to wind speed, wind direction and ambient temperature, wind density is added to the input characteristics, and the authors use Morlet wavelets as motor wavelets. The AWNN was shown to be more effective than ANNs and the adaptive neuro-fuzzy inference system (ANFIS) for wind power prediction problems.

A hybrid model combines different models that can improve forecasting accuracy by retaining each model's strengths and utilizing different aspects of data fluctuations in wind power. In the literature, a well performed hybrid model in time series forecasting tasks could capture linear and non-linear features of the time series data [21]. For example, Shi et al. [22] proposed that hybrid methods use ARIMA models to extract linear features of the data and ANN or SVM models to extract non-linear features of the data, producing two hybrid models, ARIMA-ANN and ARIMA-SVM, and comparing them with ARIMA, ANN or SVM models. Although hybrid models do not always outperform individual models, they predict better in most scenarios [4]. Therefore hybrid models are widely used for wind power forecasting. Wang et al. [23] propose a cluster hybrid wind power forecasting model called PSO-SVM-ARMA. Shetty et al. [24] propose the radial basis function neural network (RBFNN) model for wind power prediction. They use PSO to optimize the performance of the model and extreme learning machine (ELM) to improve the learning speed during training. Zameer et al. [25] propose a GPeANN model consisting of ANN and genetic programming for short-term wind power forecasting. Due to the high instability of meteorological features such as wind speed and wind direction, the predictions of individual models vary greatly. Experiments demonstrate that the proposed GPeANN model can generate a collective and robust decision space, which can avoid the above problems. Liu et al. [26] propose a new wind power prediction method using the adaptive neuro-fuzzy inference system (ANFIS) by mixing three models, which are the

backpropagation neural network (BPNN), RBFNN and least squares support vector machine (LSSVM). In order to improve the accuracy of the prediction, a method based on the Pearson correlation coefficient (PCC) is used in data pre-processing. The results show that the proposed hybrid method works better than the individual models, regardless of the season.

In recent years, deep neural networks (DNNs) have been widely used for wind power prediction, such as the convolutional neural network (CNN), long short-term memory (LSTM) and gated recurrent unit (GRU), etc. Some studies have shown that combining two or more DNNs can improve prediction results. Yu et al. [27] propose a non-parametric probabilistic prediction method based on quantile regression (QR) and the hybrid neural network (HNN) for predicting regional wind power. HNN is a special neural network obtained by mixing CNN and LSTM. It combines the advantages of CNN and LSTM models. HNN uses CNN to extract spatio-temporal features from time series data and then feeds the features into the LSTM model. Niu et al. [28] propose a sequence-to-sequence model based on the attention-based GRU (AGRU) for multi-step prediction of wind power using multiple input and output strategies. The feature selection approach evaluates the importance of each input variable by combining the attention mechanism with the GRU model. The results show that wind speed and direction impact wind power forecasting most, followed by barometric pressure and seasonal variability. A hybrid wind power forecasting method called EEMD-BA-RGRU-CSO was proposed by Meng et al. [29]. The hybrid model consists of four different models used at different stages of the experiment. Ensemble empirical mode decomposition (EEMD) is used to decompose the wind turbine power data during data pre-processing, and then the bi-attention (BA) mechanism is used for feature selection. For prediction, the RGRU model using a combination of the residual network and GRU is proposed to extract the static and dynamic relationships between features. The performance of the RGRU model is optimized at training time using the crisscross optimization algorithm (CSO). The experimental results show that the proposed hybrid method has better prediction results and is more stable than other models mentioned in the literature.

In order to improve the accuracy of wind power prediction models, many studies have used data pre-processing techniques to reduce the instability of the raw input data to better extract features. For example, combining signal decomposition algorithms such as wavelet decomposition (WD), empirical mode decomposition (EMD), EEMD and variational mode decomposition (VMD) with machine learning models. Rayi et al. [30] use the VMD algorithm to decompose historical wind power data with non-linear and non-smooth characteristics. Then they build different forecasting models for each intrinsic mode function (IMF) obtained from the decomposition, effectively improving the predicted results. Duan et al. used the vmd algorithm to decompose the wind power time series, so that the model can better extract local features [31]. LSTM and deep belief networks based on PSO were then used to construct a hybrid model for forecasting.

2.1 Contribution and paper organization

This paper focuses on medium-term wind power forecasting based on recent deep learning results. Many frameworks or methods using signal decomposition algorithms and deep learning have been proposed by many scholars, some of which also use optimization algorithms to tune the results. Among them, they provide exhaustive experiments on selecting parameters for decomposition algorithms and deep learning models on specific datasets. However, the practicality of these configurations may be limited, requiring manual re-experimentation on new data. To tackle with this situation, this paper proposes a novel medium-term forecasting framework by tree-structured parzen estimator (TPE), VMD and time fusion transformer (TFT), this framework defines the TPE-VMD-TFT method for accurate wind power forecasting. The main contributions of this study are as follows:

- (a) A novel medium-term prediction framework based on TPE and decomposition algorithms is proposed, which defines the TPE-VMD-TFT method to predict wind turbine's wind power generation

24-h and 48-h ahead. The method achieved the lowest normalized mean absolute error (nMAE) and normalized root mean square error (nRMSE) so far in the public dataset eigen.

- (b) The TPE decomposition tuning based on model (TPE-DTBM) algorithm is proposed that optimizes the parameters of the decomposition algorithm using the TPE algorithm, which can be generalized to other common decomposition algorithms and models for wind power forecasting.
- (c) The proposed framework and methodology are evaluated and analyzed from several aspects. We use nMAE, nRMSE and predictions distribution and to measure their performance on different time horizons. We evaluate both the accuracy and the stability of the proposed method.

The other subsections of the paper as follow: Section 3 describes the basic theory and signal decomposition algorithms involved in this paper. Section 4 demonstrates the validity of the proposed wind power forecasting method by using the Engie wind dataset provided by the national power corporation. Conclusions and future works are given in Section 5.

3 Methodology

3.1 LSTM

Traditional neural network cannot link the current input to historical information. In contrast, recurrent neural network (RNN) could associate contextual information and is more suitable for processing data with strong backward and forward correlations, such as time series. However, as the number of layers increases, the gradient will increase exponentially, causing the forward propagate failed and the gradient disappearing. In addition, RNNs may suffer from gradient explosion when trained with too many parameters. Gradient explosion causes the parameters to overflow, making it easier to detect than gradient disappearance. However, gradient disappearance causes the RNN model to fail in learning long-term dependency information of the time series data. To alleviate these problem, Hochreiter and Schmidhuber proposed the LSTM model, a particular type of RNN model [32]. It not only learns contextual information and long-term dependencies stored in time series data, but also overcomes the gradient disappearance problem of RNN models. The modular unit of the LSTM consists of three types of gates: input gate, output gate and forget gate. The three gates have different roles. The input gate controls the information input module cell and determines which of the current stream of information can be added to the internal state of the storage cell, which then updates the cell state. The forget gate determines which information will be discarded to preserve new information. The output gate acts in the hidden layer and controls whether the information is used as the output of the current LSTM. The gating mechanism can selectively discard irrelevant information and keep useful information, thus solving the problem of gradient dispersion in traditional RNNs.

The structure of the LSTM cell is shown in Figure 2. f_t denotes the forget gate, and the calculation formula is shown in (2). It accepts the output h_{t-1} of the previous unit and the current input x_t as input. The sigmoid function then acts to obtain a probability value (0 to 1), and information with a f_t of 0 will be discarded. i_t denotes the input gate and is calculated as shown in (1). In Equation (4), The cell state update value \tilde{c}_t is first obtained by the \tanh function and i_t by the sigmoid function. i_t can control which information from \tilde{c}_t is used to update c_t . o_t denotes the output gate and is calculated as in Equation (3). It is calculated in the same way as f_t and i_t . In Equation (5), the cell state c_{t-1} of the previous cell is obtained by dotting and summing with f_t , i_t and \tilde{c}_t to obtain the new memory cell state c_t . c_t and o_t are then calculated to obtain h_t , which is used as input to the next unit. W_i , W_f , W_o and W_c denote the weights, b_i , b_f , b_o , b_c denote the bias vectors, and σ refers to the sigmoid activation function.

$$i_t = \sigma (W_i \times [h_{t-1}, x_t] + b_i) \quad (1)$$

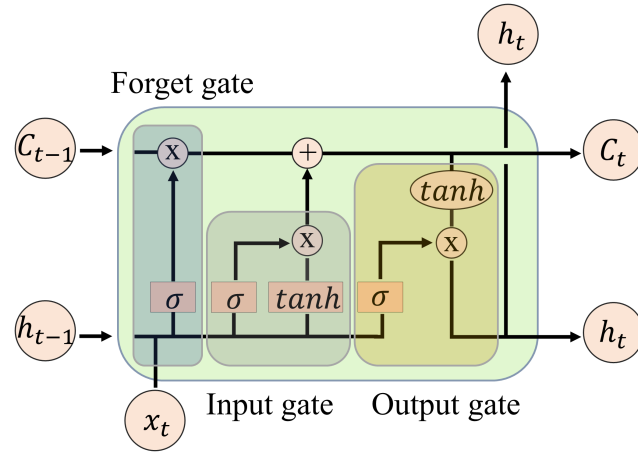


Figure 2. LSTM network structure diagram.

$$f_t = \sigma(W_f \times [h_{t-1}, x_t] + b_f) \quad (2)$$

$$o_t = \sigma(W_o \times [h_{t-1}, x_t] + b_o) \quad (3)$$

$$\tilde{c}_t = \tanh(W_c \times [h_{t-1}, x_t] + b_c) \quad (4)$$

$$c_t = f_t \times c_{t-1} + i_t \times \tilde{c}_t \quad (5)$$

3.2 XGBRegressor

Unlike ANN, LSTM and CNN, which belong to strong learner, the eXtreme Gradient Boosting (XGBoost) algorithm proposed by Chen et al. is a Boosting algorithm with multiple learners [33]. This kind of algorithm is an essential branch of integration learning, where a strong learner is obtained by assigning different weights to multiple weak learners according to their accuracy. An important application of Boosting algorithms to solve regression problems is gradient boosting decision tree (GBDT), which obtains a target regressor by integrating multiple decision trees. In GBDT, each decision tree is built toward the decreasing model's loss. The loss value of adding trees in each round is fitted by the negative gradient of the loss function, which is the same principle as Adaboost in the Boosting algorithm. Such algorithms could satisfy both classification tasks and regression tasks, thus their subtrees are generally classification and regression trees (CART), which are built recursively to build binary trees that are optimal by the definition of the algorithm.

XGBoost is an improvement and excellent practice of the GBDT algorithm, which adds a regularisation term to the GBDT objective function that related to the node partitioning difficulty factor and tree size, It controls the tree size to reduce the possibility of overfitting and speeding up the convergence of the algorithm. In addition, second-order Taylor expansions can make the loss function accurate and allow the function to converge in a precise direction. As one of the few integrated learning algorithms that can compete with strong learners, many researchers have conducted further studies such as missing value processing and feature importance analysis to the XGBoost algorithm, making it valuable for practical problems. XGBoost that handling regression problems is referred as the XGBRegressor.

3.3 TFT

TFT is a deep neural network architecture based on the attention mechanism which is proposed by Lim et al. and widely used in time series data prediction [34]. The model architecture of the TFT is shown in Figure 3. Compared to other artificial intelligence-based models, the TFT model has a much-improved performance with greater interpretability. The TFT model classifies input features into different types, including static covariates, future inputs that can be speculated and time series data that are known in the past but not known in the future. It also captures the interactions between different types of input features in multi-horizon forecasting and estimates the importance of these features to the forecasting outcome.

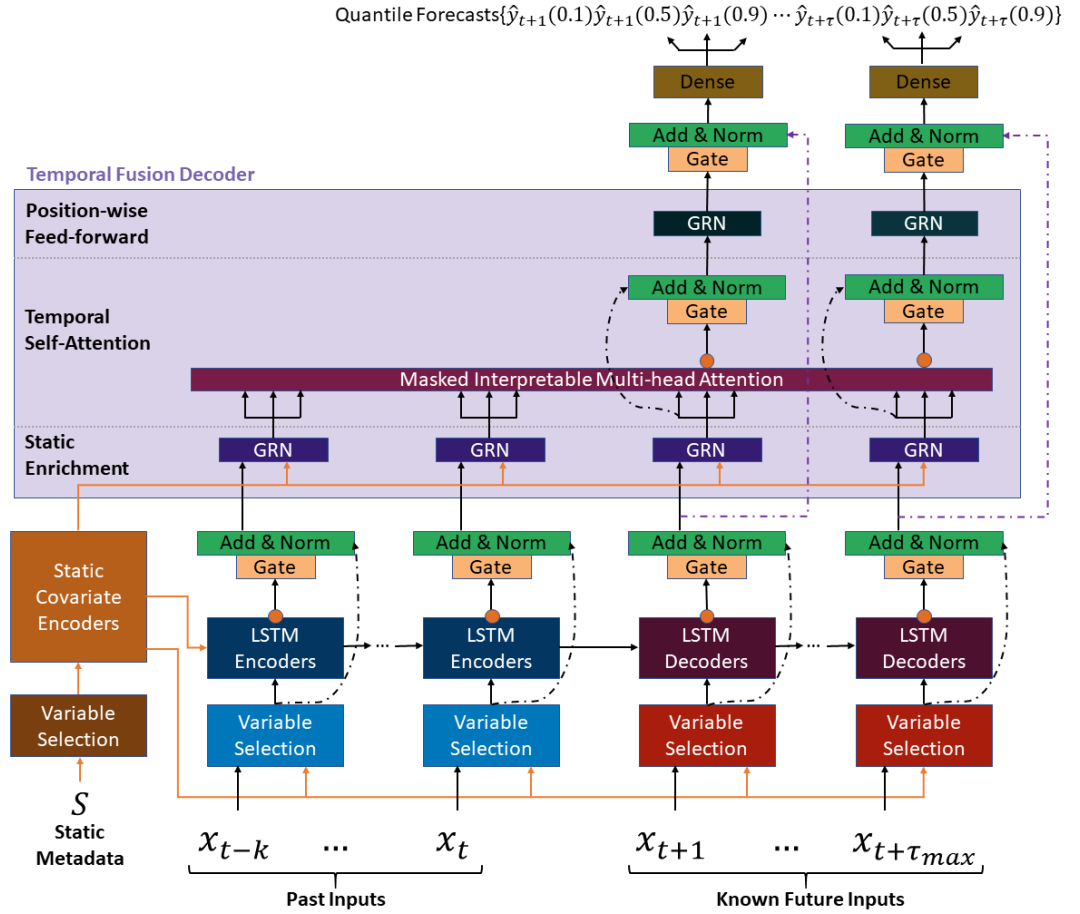


Figure 3. The model architecture of TFT.

$$\hat{y}_i(q, t, \tau) = f_q(\tau, y_{i,t-k:t}, o_{i,t-k:t}, k_{i,t-k:t+\tau}, s_i) \quad (6)$$

The multi-step prediction function is defined as shown in Equation (6). In wind power forecasting, i denotes a different wind farm, and t denotes a different point in time. s_i denotes a static variable that does not change over time, and $y_{i,t}$ denotes the target variable for prediction. The time-related dynamic variables represented by $x_{i,t} = [o_{i,t}, k_{i,t}]$ can be divided into two categories. $o_{i,t}$ indicates variables that change over time which are not known in advance, such as meteorological data (e.g., wind speed, wind direction, temperature, etc.). The variables indicated by $k_{i,t}$ change over time but can be inferred from known conditions, such as weeks, months, seasons and special holidays, etc. In addition, f_q denotes the model used for forecasting and the function expresses the value of quantile q at time t for forecasting the future at step τ . Unlike classic regression models,

TFT uses quantile loss instead of the traditional MSE loss. That allows the TFT to fit multiple target regions in high-dimensional space. According to the definition of quantile loss, the quantile q takes on a value between 0 and 1. Usually, when different q are chosen, there is an imbalance between positive and negative errors in the loss function. Therefore, quantile loss can avoid overfitting and underfitting the model and achieve quantile regression. The TFT model uses the quantile group Q and obtains the final loss by weighted summing all q in Q .

The TFT model consists of several modules with different purpose, which can extract features from various types of input data. (1) The function of gating mechanisms is to forget unnecessary parts, which not only simplifies the structure of the model, but also improves the performance of the model on different tasks. (2) Variable selection networks identify important input features at each time step, which can alleviate the problem of traditional DNNs over-fitting and predicting features with irrelevant targets, and improve the ability of the model to adapt to different samples. (3) Static covariate encoders moderate the temporal dynamics modeling by encoding static features, as static information may be important for predicting the target, which helps to improve the prediction results. (4) Temporal processing enables the model to learn long and short-term time dependencies from future inputs obtained through speculation and from time series data that are known in the past but not in the future. This part consists of two modules, the sequence-sequence layer and the multi-headed attention layer, which perform local processing and learn long-term dependencies. (5) Prediction intervals show quantile predictions helpful in understanding the output distribution.

Gating mechanisms

In the field of time series forecasting, there are data sets of varying sizes and quality. In order to make the TFT model more generalizable and adaptable to realistic and complex scenarios, the gated residual network (GRN) is used to address the complexity of the input time series data. When encountering small and noisy datasets, there is no need for more complex models. GRN provides the flexibility to control the degree of non-linear transformation applied to improve model prediction. The GRN is defined as shown in Equation (7). Its input consists of two types, the primary input data \mathbf{a} and the optional context vector \mathbf{c} . In Equation (9), ELU is the activation function. Its may take negative values. In addition, it allows the unit activation means to be closer to 0 than other linear unsaturated activation functions (such as ReLU). [35].

$$\text{GRN}_\omega(\mathbf{a}, \mathbf{c}) = \text{LayerNorm}(\mathbf{a} + \text{GLU}_\omega(\boldsymbol{\eta}_1)) \quad (7)$$

$$\boldsymbol{\eta}_1 = \mathbf{W}_{1,\omega}\boldsymbol{\eta}_2 + \mathbf{b}_{1,\omega} \quad (8)$$

$$\boldsymbol{\eta}_2 = \text{ELU}(\mathbf{W}_{2,\omega}\mathbf{a} + \mathbf{W}_{3,\omega}\mathbf{c} + \mathbf{b}_{2,\omega}) \quad (9)$$

The GLU can control the degree of non-linear transformation and improve the model's flexibility. It is defined as shown in Equation (10). $\boldsymbol{\gamma}$ denotes the input, \mathbf{W} and \mathbf{b} denote the weights and bias, and $\sigma(\cdot)$ denotes the sigmoid activation function. The output of the sigmoid function is between 0 and 1 and serves to perform feature selection. The GLU is a crucial part of the GRN's implementation function. When the input is small-scale data, a simple non-linear transformation may be required when the GLU can achieve this by outputting a vector close to 0.

$$\text{GLU}_\omega(\boldsymbol{\gamma}) = \sigma(\mathbf{W}_{4,\omega}\boldsymbol{\gamma} + \mathbf{b}_{4,\omega}) \odot (\mathbf{W}_{5,\omega}\boldsymbol{\gamma} + \mathbf{b}_{5,\omega}) \quad (10)$$

Variable selection networks

When the model has multiple input variables, it is difficult to determine the importance of target vector in prediction. The TFT model proposes Variable selection networks for variable input selection. However, instead of directly discarding features that do not contribute to the prediction results, it weights the input variables. Higher weights indicate higher levels of importance. That not only mitigates the negative impact of unimportant feature vectors, but also improves the performance of the model.

$$v_{\chi_t} = \text{softmax}\left(\text{GRN}_{v_{\chi}}(\Xi_t, c_s)\right) \quad (11)$$

$$\tilde{\xi}_t = \sum_{i=1}^{m_x} v_{\chi_t}^{(i)} \tilde{\xi}_t^{(i)} \quad (12)$$

$$\tilde{\xi}_t^{(i)} = \text{GRN}_{\tilde{\xi}^{(i)}}\left(\xi_t^{(i)}\right) \quad (13)$$

Variable selection networks utilize GRN to each feature individually, then concatenate the features before inputting to the GRN again. Softmax is also used to generate feature weights, assigning the resulting weights to different input variables. The way to obtain the weights is shown in Equation (11). Equation (12) represents the combination method for weighting the features, where $v_{\chi_t}^{(i)}$ is the weight of the feature selection, and $\tilde{\xi}_t^{(i)}$ is the feature after the GRN non-linear processing. The formula for calculating $\tilde{\xi}_t^{(i)}$ is represented in Equation (13).

Static covariate encoders

TFT produces four output variables cs , cc , ch and ce using four different GRNs. (1) temporal variable selection (cs) as the input to Variable selection networks. (2) local processing of temporal features (cc , ch), input LSTM as initialization state. (3) enriching temporal features with static information (ce) and input into the Static Enrichment.

Interpretable multi-head attention

The interpretable multi-head attention module of the TFT model is based on the transformer model of multi-head attention, as shown in Equations (14)-(15). In the transformer model, the multi-headed attention mechanism forms multiple subspaces by dividing the model into multiple heads. Each head learns different weights, which facilitates the model to learn different aspects of the features. Better predictions can be achieved by collecting these features, but they are challenging to interpret. To increase interpretability, the TFT model modifies the v matrix of each head to share weights, while the Q and K matrices do not share weights as before.

$$\text{InterpretableMultiHead}(Q, K, V) = \tilde{H}W_H \quad (14)$$

$$\begin{aligned} \tilde{H} &= \tilde{A}(Q, K)VW_V \\ &= \left\{ \frac{1}{m_H} \sum_{h=1}^{m_H} A\left(QW_Q^{(h)}, KW_K^{(h)}\right) \right\} VW_V \\ &= \left\{ \frac{1}{m_H} \sum_{h=1}^{m_H} \text{Attention}\left(QW_Q^{(h)}, KW_K^{(h)}, VW_V\right) \right\} \end{aligned} \quad (15)$$

3.4 Signal decomposition algorithms

EEMD

EMD is a method proposed by Huang et al. to decompose signals [36]. EMD can decompose the original signal, which reflects the time-scale characteristics of the data, into several intrinsic mode functions (IMFs), but the frequencies of these IMF components may differ. It is often the case that an IMF may contain feature components at different time scales, leading to the problem of mode mixing in EMD. To avoid the mode mixing problem between IMFs, Wu and Huang developed an improved method for EMD, the EEMD algorithm [37]. EEMD takes advantage of white noise having a zero average value, and changes the extreme value point of the signal by adding Gaussian white noise several times during the EMD decomposition process. After several averaging processes, the noises cancel each other out. The more averaging times, the less noise is introduced into the decomposition and the less impact on the result [38].

VMD

The VMD algorithm is a signal processing algorithm based on wiener filtering, Hilbert transform and frequency mixing [39]. The VMD algorithm is adaptive and non-recursive. Adaptive is the algorithm's ability to determine the number of mode decompositions based on the actual problem and to match each mode component's optimum center frequency and bandwidth during the operation. Compared to the EMD algorithm, it has a better mathematical theoretical basis and can separate signals accurately and efficiently. The VMD algorithm is applied to highly complex, strongly non-linear time series to reduce non-smoothness. The decomposition results in several relatively smooth subseries, effectively eliminating the effect of noise and allowing the capture of essential features of the original signal. The VMD algorithm can decompose the multi-component signals $f(t)$ into k mode state quantities $u_k(t)$. The central frequency $w_k(t)$ of each mode state quantity $u_k(t)$ is of a specific bandwidth. The expression for the constraint variable is shown in Equation 16, where $\delta(t)$ denotes the Dirac function and $*$ denotes the convolution operator. The Equation shows that all modes' sum equals the original signal f . When the estimated central frequency $w_k(t)$ is reasonably limited, reducing the frequency overlap problem between different modes is beneficial.

$$\min_{\{u_k\}, \{\omega_k\}} \left\{ \sum_k \left\| \partial_t \left[\left(\delta(t) + \frac{j}{\pi t} \right) * u_k(t) \right] e^{-j\omega_k t} \right\|_2^2 \right\} \text{ s.t. } \sum_k u_k = f \quad (16)$$

MSTL

Cleveland et al. proposed the seasonal-trend decomposition based on loess (STL) algorithm [40]. STL is often used to decompose a time series into a single seasonal component, decomposing it into a sum of trend, seasonality and residuals. In order to extract multiple seasonal cycles of a time series, K. Bandara et al. proposed the multiple seasonal-trend decomposition based on loess (MSTL) decomposition algorithm based on STL [41]. After MSTL extracts the multiple seasonal components of the time series based on ascending iterations, the trend and residuals are obtained by a final iteration.

3.5 Optimize parameters with optuna

There are many papers on automatic parameter tuning of decomposition algorithms in wind power forecasting research. For example, An et al. proposed a PVMD algorithm that uses PSO to optimize the critical parameters of VMD $[K, \alpha]$ [42]. Yu et al. use the whale algorithm adaptively optimize the critical parameters of the VMD [43]. Li et al. use the flower pollination algorithm to optimize the parameters of the VMD automatically and specify the decomposition loss as the criterion for evaluating the optimal parameters [44]. In these articles, the optimization VMD algorithm is inde-

pendent of the prediction model. The evaluation criteria guiding the tuning of the parameters vary, resulting in the final optimal parameters not necessarily being suitable for the specific prediction model. Therefore, we propose an algorithm for parameter selection of the critical parameters of the decomposition algorithm forecasting models.

Optuna is an open-source hyperparametric optimization framework that enables automatic and efficient tuning of machine learning and deep learning algorithms [45]. It contains many tuning algorithms (such as grid search, stochastic search and Bayesian optimization algorithms) to find the optimal solution to the problem automatically. Thus optuna can be applied to the tuning of most machine learning models. Optuna offers two main samplers with different functions: the covariance matrix adaptation evolution strategy (CMA-ES) samples the relationships between parameters, and the TPE samples the parameters independently.

The algorithm uses the TPE to optimize the parameters of the signal decomposition, the flow is shown in Figure 4. First, a signal decomposition algorithm is selected and the intervals of its critical parameters are estimated based on the study [37, 39]. The TPE algorithm is then used to select the possible values of the critical parameters, input them into the prediction model for training, and calculate the prediction error. Then, determine if the prediction error has changed. If the prediction error is reduced, then the optimal value of the parameter is updated, and the process moves on to the next step. If the prediction error has not changed or has improved, skip to the next step. In the end, determine if the upper limit of the iteration has been reached. If not reached, then jump to the TPE optimizer and continue the loop to optimize the values of the parameters. If the iteration termination condition is met, the optimal value of the critical parameter is output.

4 Data description and evaluation metrics

4.1 Data description

We use the dataset from the La Haute Borne wind farm in Meuse, France, with a longitude of 5.6013 E and a latitude of 48.4503 N. Meuse is located on the west coast of the ocean and has an oceanic climate with an average annual temperature of 11.36°C. There is narrow annual temperature range and few extremes of temperature, with warm summers and cool winters. It is rich in wind energy and has high wind speeds due to the influence of the Atlantic sea breeze.

The dataset uses the Engie wind dataset provided by the electricity company in France [46]. The dataset is derived from the SCADA system and records daily electricity production from 2012 to 2018 for four wind power turbines rated at 2 MW. Data from 2012 to 2015 were used as training data, the data from 2016 as the validation set, and data from 2017 and 2018 were used as test data. Each wind turbine has three features: power, wind turbine and meteorology data. The power features include active power, reactive power and apparent power. The wind turbine data include a total of twenty-two features such as converter torque, generator converter speed and pitch angle, etc. The meteorology features include outdoor temperature, wind speed, and absolute wind direction. Each feature has average, minimum, maximum and stand-deviation values. The data set has 0.02% to 0.05% missing cells and 0.65% to 0.88% missing records. The missing values are shorter than one day, so we fill them with near day in similar weather conditions. For the very rare outliers (e.g., minus 10 degrees never happens in Grand Est), we replace them with the corresponding extrema values. The interval between data readings is 10 minutes. Due to the high instability of wind data, too much data density makes prediction more difficult. Therefore, we resampled the data and changed the resolution of the dataset to one hour.

The correlation between wind power production and meteorological variables varies according to geographical location. The correlation between wind power production and wind speed is more significant than other meteorological variables at the La Haute Borne wind farm. Figure 5 shows wind power and wind speed scatter plots from the raw data collected from the four wind farms.

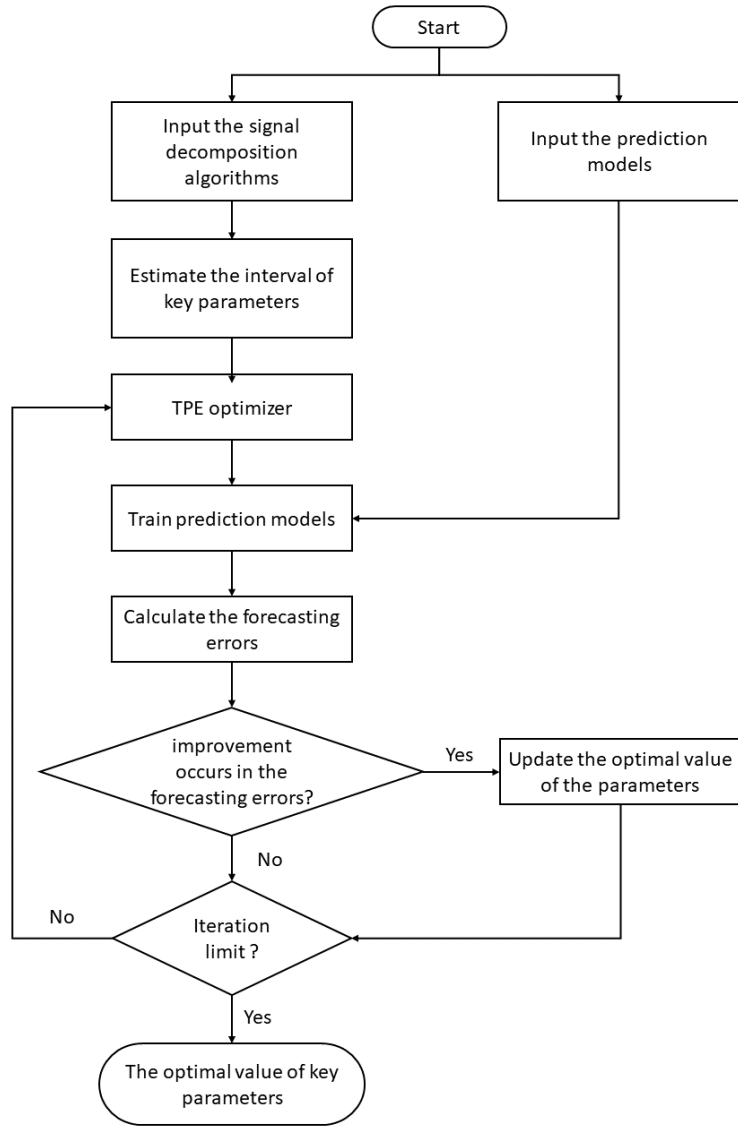


Figure 4. Flow chart for optimizing VMD parameters based on the TPE.

Figure 6 shows the scatter plot obtained by dividing the data according to the different months. These figures show a progressive increase in the cluster of points around the diagonal, indicating a strong correlation between wind power and wind speed.

4.2 Evaluation Metrics

In order to evaluate the performance of the proposed method, the following two metrics of statistical prediction and actual value error were used: nMAE and nRMSE. They normalize loss as percentages to illustrate the error range, which allows comparison of different wind turbines. And nMAE use absolute error to prevent losses from offsetting, with low sensitivity to outliers. nMAE and nRMSE are defined as shown below.

$$nRMSE = \sqrt{\frac{1}{T y_{max}^2} \sum_{i=1}^T (y_i - \hat{y}_i)^2} \quad (17)$$

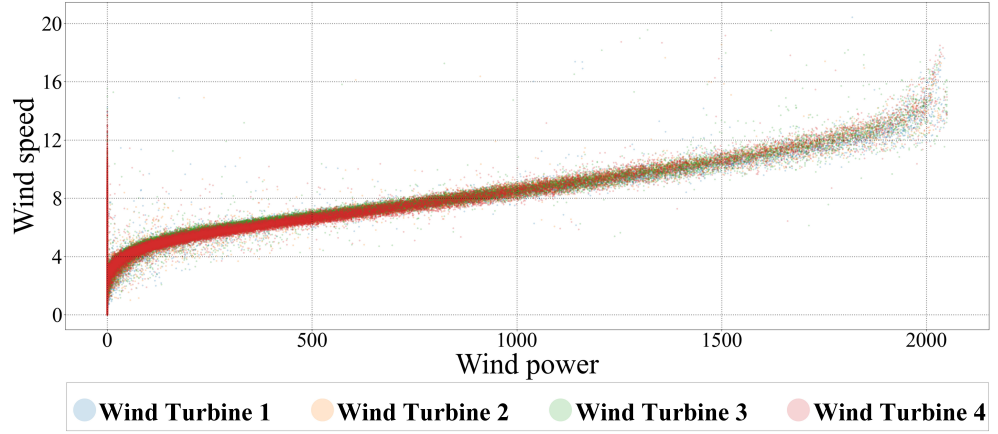


Figure 5. Scatter plot of wind power and wind speed from raw data

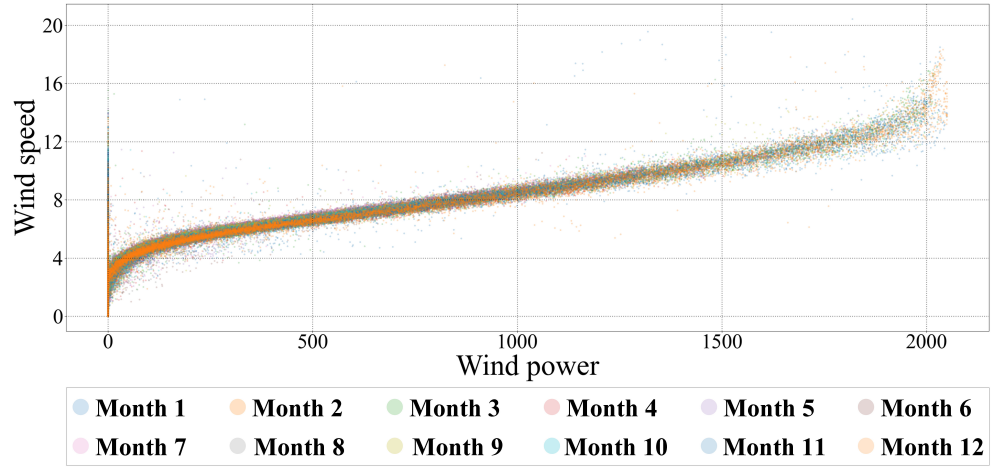


Figure 6. Scatter plot of wind power and wind speed according to different months

$$nMAE = \frac{1}{T y_{max}} \sum_{i=1}^T |y_i - \hat{y}_i| \quad (18)$$

Where T denotes the forecast length, y_i denotes the actual wind power at point i , \hat{y}_i is the predicted value of wind power at point i , and y_{max} denotes the maximum value of the actual wind power. In wind power forecasting studies, the units of RMSE and MAE can be kW, kWh and percentage, depending on the forecast object. In this paper, the units of each evaluation metric are in percentages to allow comparison with other wind power forecasting models.

4.3 Signal decomposition algorithm to decompose wind power sequences

Wind power generation data has intense instability and intermittent time series data. The regularity the series is not obvious and not easy to detect patterns through observation. Similarly, it is difficult for prediction models to obtain accurate predictions from the raw data. To solve this problem, many studies have used signal decomposition algorithms on wind power sequences to obtain a

number of subsequences with stronger regularity. The sum of the subsequences is equal to the original sequence and they are more predictable. So signal decomposition algorithms are common in wind power prediction.

We use EEMD to decompose the wind power series to obtain three IMFs (including trend and two subs) and a trend-residual, as shown in Figure 7. The decomposed wind power generation data is less volatile and random, and the IMFs have some regularity, which helps to improve the accuracy of wind power forecasting.

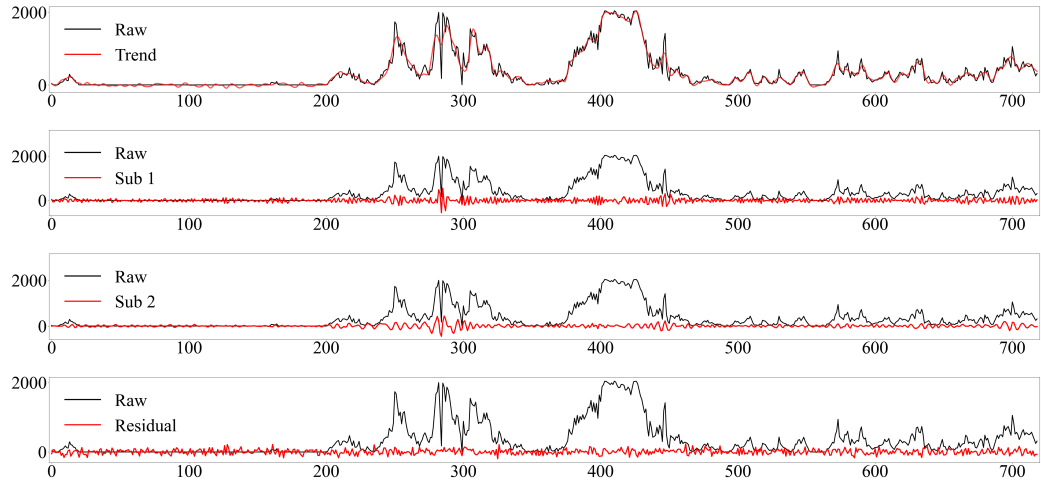


Figure 7. EEMD algorithm decomposes wind power data

The VMD decomposition algorithm is an effective method to solve the mode conflation problem that occurs in EEMD. The decomposition results are shown in Figure 8. The decomposition results in three IMFs around a central frequency and a residual, which adaptively separates the IMFs in different frequency bands.

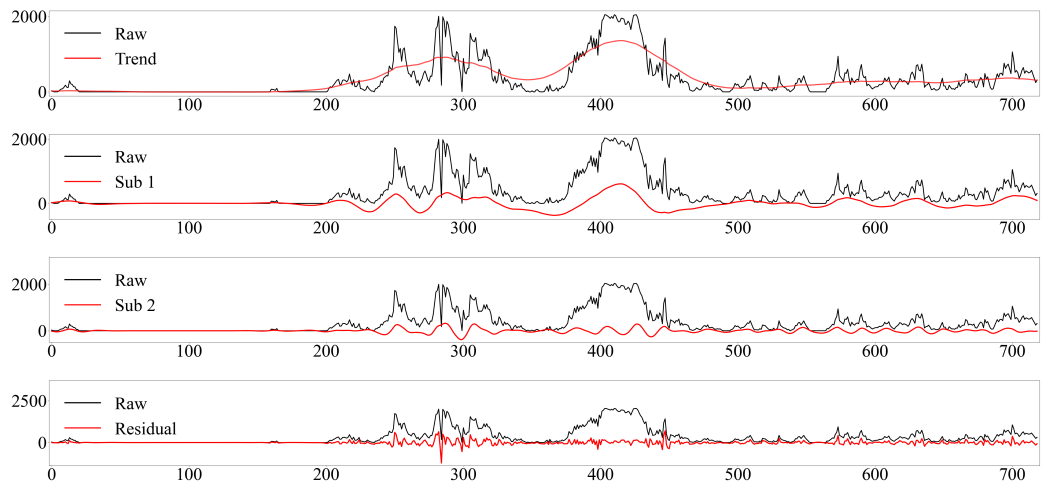


Figure 8. VMD algorithm decomposes wind power data

Unlike the EEMD and VMD algorithms, MSTL is a time series decomposition algorithm that can reflect the patterns and cycles of wind power generation over time. The MSTL method was used to decompose the original wind power sequence, and the results are shown in Figure 9. As can be seen from the figure, decomposing the original series yields a trend, two period series and a

residual, which extracts the multiple seasonal trends of the series.

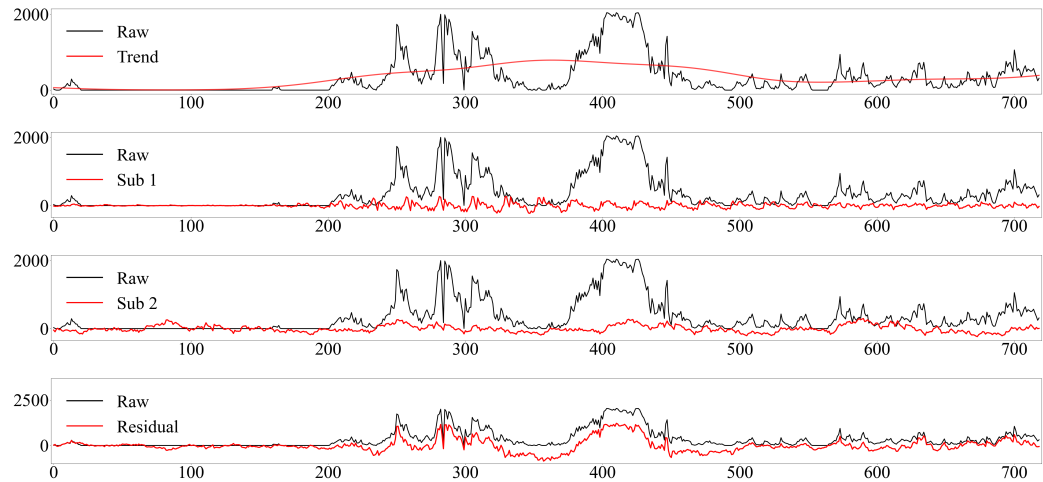


Figure 9. MSTL algorithm decomposes wind power data

The low-frequency components represent the original data's overall trend, and the high-frequency components represent the local trend. As can be seen, the trend of EEMD is very close to the original data, similar to the smoothed data of the original data. However, the other parts are more frequent. VMD's trend is not close to the original data but is lower in all parts of the frequency. MSTL only has a relatively low frequency for trend, the other components have a high frequency, and the residuals are very close to the original data.

4.4 Experimental results and analysis

The machine learning models adopted in this section implemented by Python 3.8 and Torch 1.13.1, Pytorch-forecasting 0.10.2 and Pytorch-lightning 1.7.2. This paper uses historical data collected from the SCADA system of the engine wind farm. All models use the "TimeSeriesDataSet" for data pre-processing and early stopping to prevent over-fitting of the models. The performance of the proposed new framework is verified by nMAE, nRMSE and stability analysis.

The TFT model performs optimally under the same decomposition algorithm conditions in the proposed framework. Here we list the parameters derived for each decomposition algorithm in the framework of the used TFT model. The parameters used for TPE-EEMD are: trials are 93, noise_width is 0.05 and MAX_IMF is 13; The parameters used for TPE-VMD are: alpha is 5700 and K is 30; The parameters used for TPE-MSTL are: periods are 6 and 48. The other hyperparameters are: the hidden layers are set as 11, the learning rate is set to 0.004, and the batch size is 32. In addition, the optimal parameters for the decomposition algorithms of ANN, LSTM, CNN-LSTM, RNN-LSTM and XGB models are also derived from this framework. Since they are not the focus of this paper.

In this study, TPE-VMD-TFT outperforms other methods. We have chosen two interval lengths of 24h and 48h for the prediction time. Here we first compare TPE-VMD-TFT with the individual model, and then compare TPE-VMD-TFT and models based on the proposed framework. Next, we verified the validity of the model's predictions by analyzing the performance of TPE-VMD-TFT in different months, seasons and years.

Comparison of TPE-VMD-TFT and individual models

ANN, LSTM, CNN-LSTM, RNN-LSTM, XGB and TFT are commonly used for wind power prediction. Here we compare them with the proposed TPE-VMD-TFT method as in Table 1. In TPE-VMD-TFT, VMD optimizes the parameters by TFT, which uses the data decomposed by VMD for training and

Table 1. TPE-VMD-TFT method and other models for 24-h and 48-h ahead prediction error results.

Model	Wind Turbine 1				Model	Wind Turbine 2			
	24-h		48-h			24-h		48-h	
	nMAE	nRMSE	nMAE	nRMSE		nMAE	nRMSE	nMAE	nRMSE
ANN	14.34%	18.31%	18.42%	21.64%	ANN	13.65%	17.31%	15.47%	18.96%
LSTM	12.94%	17.95%	17.02%	27.00%	LSTM	11.89%	16.79%	16.11%	25.14%
CNN-LSTM	12.83%	19.53%	14.97%	22.50%	CNN-LSTM	11.94%	17.33%	13.84%	20.82%
RNN-LSTM	12.73%	18.02%	15.15%	22.27%	RNN-LSTM	12.20%	16.94%	14.01%	20.56%
XGB	12.63%	17.58%	15.10%	19.97%	XGB	11.61%	16.31%	13.81%	18.45%
TFT	11.93%	17.58%	16.06%	23.00%	TFT	11.41%	16.74%	14.28%	20.04%
TPE-VMD-TFT	4.26%	6.59%	7.33%	10.87%	TPE-VMD-TFT	4.02%	6.21%	7.50%	10.78%
Model	Wind Turbine 3				Model	Wind Turbine 4			
	24-h		48-h			24-h		48-h	
	nMAE	nRMSE	nMAE	nRMSE		nMAE	nRMSE	nMAE	nRMSE
ANN	16.11%	19.53%	20.77%	23.74%	ANN	17.42%	20.30%	19.55%	22.53%
LSTM	15.36%	19.63%	19.91%	29.47%	LSTM	14.56%	18.51%	18.98%	27.49%
CNN-LSTM	14.94%	19.65%	16.73%	23.62%	CNN-LSTM	14.05%	18.90%	17.80%	28.13%
RNN-LSTM	13.87%	19.05%	16.96%	23.27%	RNN-LSTM	13.81%	18.28%	15.85%	22.48%
XGB	14.73%	18.95%	17.33%	21.56%	XGB	13.47%	18.08%	15.60%	20.19%
TFT	15.78%	20.20%	17.15%	23.51%	TFT	13.92%	19.05%	15.18%	22.46%
TPE-VMD-TFT	4.63%	6.78%	7.99%	11.59%	TPE-VMD-TFT	4.59%	6.75%	7.35%	10.83%

prediction. Individual models use the original wind power sequence data for training and prediction.

As can be seen from the table, the nMAE and nRMSE of the TPE-VMD-TFT model are smaller on the wind power data from all four turbines compared to the individual models. In 24-h ahead wind power forecasting, the values of nMAE for the TPE-VMD-TFT model are 4.26%, 4.02%, 4.63% and 4.59%. The prediction results at wind turbine 1 are 70.29%, 67.08%, 66.80%, 66.54%, 66.27% and 64.29% lower than the prediction errors of the ANN, LSTM, CNN-LSTM, RNN-LSTM, XGB and TFT models. Similarly, its values for nRMSE were 6.59%, 6.21%, 6.78% and 6.75%. The prediction results at wind turbine 1 were 64.01%, 63.29%, 66.26%, 63.43%, 62.51% and 62.51% lower than the prediction errors of the individual models. The TPE-VMD-TFT model predicted the 48-h ahead with values of 7.33%, 7.5%, 7.99% and 7.35% for nMAE. The prediction results in wind turbine 1 were 60.21%, 56.93%, 51.04%, 51.62%, 51.46% and 54.36% lower than the prediction errors of ANN, LSTM, CNN-LSTM, RNN-LSTM, XGB and TFT models. Similarly, its values for nRMSE were 10.87%, 10.78%, 11.59% and 10.83%. The prediction results at wind turbine 1 were 49.77%, 59.74%, 51.69%, 51.19%, 45.57% and 52.74% lower than the prediction errors of the individual models. Even the forecasting model is same, the TPE-VMD-TFT method was significantly better than the TFT. This maybe because the TPE-VMD-TFT method uses an optimized VMD to decompose the wind power series, producing smoother IMFs compared to the original data (subsection 4.3) and reducing the effect of noise on the prediction results. Thus, regarding overall results, TPE-VMD-TFT significantly outperforms other individual models.

We draw scatter plots to compare the prediction performance of the individual model and TPE-VMD-TFT on each day in the test set. Using the 24h prediction as an example, Figure 10 represents the predicted and actual values for the TPE-VMD-TFT model and other models on the four wind turbines. The horizon axis represents the actual value of wind power, and the vertical axis represents the model's predicted value. The red diagonal indicates the ideal prediction, the yellow dots indicate the TPE-VMD-TFT model and the blue dots indicate other models. As can be seen from the figure, the yellow points are mainly distributed around the diagonal. In contrast, the blue points are more dispersed, indicating that the proposed TPE-VMD-TFT model has a higher accuracy rate than the individual models. For the ANN and XGB models, we found that the points they predicted

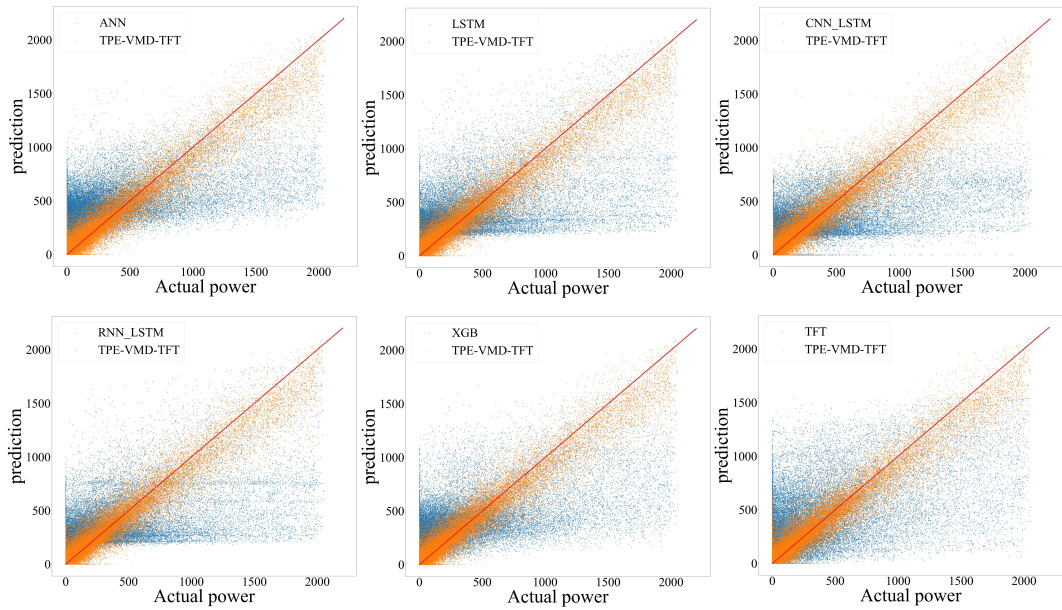


Figure 10. Scatter plot of the models' predicted and actual values on four wind turbines.

were located above the diagonal and closer to the origin of the coordinates, suggesting that they were biased towards higher predictions for lower power. For the LSTM, CNN-LSTM and RNN-LSTM models, we find that many prediction points are distributed in a region parallel to the horizontal axis, suggesting that they predict them as the same range of values for some point, regardless of the actual value. No significant aggregation areas emerged for the TFT model alone, and its points in high power is scattered. We can therefore see that ANN, LSTM, CNN-LSTM, RNN-LSTM and XGB produce certain fixed output patterns to fit the training metrics in the complex raw wind power data. However, the TFT and XGB model does not produce this pattern. In addition, we find that the individual models have very few points in the upper right region of the scatter plot, indicating that they are poor predictors of peak power. For the TPE-VMD-TFT model, we find that the prediction points are almost evenly distributed on both sides of the ideal prediction, and there are also more points in the peak region, with less dispersion in the upper right point than in the lower left. By comparison, we can find that the TPE-VMD-TFT model has the best prediction at low power compared to other individual models. Furthermore, at high power, although the prediction error is higher than at low power, it is a significant improvement over the other models.

Comparison of TPE-VMD-TFT and models based on the proposed frame

The proposed TPE-VMD-TFT performed much better than the other individual models in the previous subsection. At the same time, the decomposition algorithm significantly impacts the accuracy of the prediction. For example, the TFT in the previous subsection has a lower prediction than the TPE-VMD-TFT. Therefore, the algorithm used in our TPE-VMD-TFT generalized to other individual models so that they can also be trained and predicted using the optimized decomposition algorithm. Therefore, the algorithm used in our TPE-VMD-TFT generalizes to other individual models so that they can also be trained and predicted using the optimized decomposition algorithm. In this subsection, we compare and analyze TPE-VMD-TFT with other individual models based on the proposed frame. The comparison method includes all the decomposition algorithms and models mentioned earlier: TPE-EEMD-ANN, TPE-EEMD-LSTM, TPE-EEMD-CNN-LSTM, TPE-EEMD-RNN-LSTM, TPE-EEMD-XGB, TPE-EEMD-TFT, TPE-VMD-ANN, TPE-VMD-LSTM, TPE-VMD-CNN-LSTM, TPE-VMD-RNN-LSTM, TPE-VMD-XGB, TPE-MSTL-ANN, TPE-MSTL-LSTM, TPE-MSTL-CNN-LSTM, TPE-MSTL-RNN-

model	Wind Turbine 1											
	24-h						48-h					
	TPE-EEMD		TPE-VMD		TPE-MSTL		TPE-EEMD		TPE-VMD		TPE-MSTL	
	nMAE	nRMSE	nMAE	nRMSE	nMAE	nRMSE	nMAE	nRMSE	nMAE	nRMSE	nMAE	nRMSE
ANN	7.57%	10.65%	7.27%	9.37%	10.34%	12.75%	16.55%	20.35%	15.97%	18.51%	17.28%	20.06%
LSTM	7.75%	10.84%	5.98%	8.96%	11.66%	15.84%	16.34%	25.56%	17.61%	27.37%	17.61%	27.31%
CNN-LSTM	8.60%	12.29%	6.23%	9.22%	11.13%	16.11%	14.85%	22.18%	14.66%	22.12%	14.87%	22.70%
RNN-LSTM	8.75%	12.76%	7.07%	9.78%	12.05%	15.48%	15.62%	21.95%	15.20%	22.22%	15.11%	22.30%
XGB	8.41%	12.34%	7.17%	10.87%	11.92%	16.46%	10.63%	14.98%	10.23%	14.80%	14.66%	19.37%
TFT	6.82%	10.15%	4.26%	6.59%	10.68%	15.31%	8.95%	12.82%	7.33%	10.87%	13.19%	19.41%
model	Wind Turbine 2											
	24-h						48-h					
	TPE-EEMD		TPE-VMD		TPE-MSTL		TPE-EEMD		TPE-VMD		TPE-MSTL	
	nMAE	nRMSE	nMAE	nRMSE	nMAE	nRMSE	nMAE	nRMSE	nMAE	nRMSE	nMAE	nRMSE
ANN	7.72%	10.40%	6.27%	8.26%	9.39%	11.45%	13.82%	18.20%	10.38%	13.34%	16.02%	18.61%
LSTM	7.46%	10.28%	6.08%	8.89%	10.27%	15.07%	15.92%	24.63%	17.68%	26.13%	18.32%	26.61%
CNN-LSTM	7.84%	11.13%	5.73%	8.33%	10.97%	15.01%	13.91%	20.72%	13.54%	20.40%	13.83%	20.93%
RNN-LSTM	8.39%	12.25%	5.91%	8.43%	12.27%	15.50%	14.47%	20.20%	14.12%	20.41%	14.47%	20.26%
XGB	7.62%	11.29%	6.83%	10.21%	11.10%	15.49%	9.74%	13.85%	9.64%	13.71%	14.01%	18.49%
TFT	6.55%	9.55%	4.02%	6.21%	9.41%	14.13%	9.89%	14.10%	7.50%	10.78%	12.12%	17.35%
model	Wind Turbine 3											
	24-h						48-h					
	TPE-EEMD		TPE-VMD		TPE-MSTL		TPE-EEMD		TPE-VMD		TPE-MSTL	
	nMAE	nRMSE	nMAE	nRMSE	nMAE	nRMSE	nMAE	nRMSE	nMAE	nRMSE	nMAE	nRMSE
ANN	10.49%	13.16%	10.87%	12.91%	11.12%	13.58%	22.43%	25.33%	17.71%	20.23%	19.44%	22.47%
LSTM	9.29%	11.76%	7.74%	10.21%	11.99%	16.79%	19.75%	29.02%	19.66%	29.05%	20.03%	29.52%
CNN-LSTM	9.23%	12.60%	8.00%	10.29%	12.90%	17.07%	16.04%	22.59%	16.50%	23.55%	16.63%	23.81%
RNN-LSTM	9.36%	13.22%	9.08%	11.04%	13.26%	16.64%	17.82%	22.92%	17.24%	23.12%	17.07%	23.18%
XGB	9.56%	13.01%	8.17%	11.36%	12.65%	16.93%	12.02%	15.80%	11.83%	15.56%	15.82%	20.18%
TFT	7.62%	11.06%	4.63%	6.78%	10.59%	15.13%	10.25%	13.73%	7.99%	11.59%	14.95%	21.04%
model	Wind Turbine 4											
	24-h						48-h					
	TPE-EEMD		TPE-VMD		TPE-MSTL		TPE-EEMD		TPE-VMD		TPE-MSTL	
	nMAE	nRMSE	nMAE	nRMSE	nMAE	nRMSE	nMAE	nRMSE	nMAE	nRMSE	nMAE	nRMSE
ANN	10.37%	12.79%	7.98%	10.07%	10.62%	13.24%	18.20%	21.51%	13.36%	16.16%	17.59%	20.30%
LSTM	8.00%	11.10%	6.48%	9.57%	11.09%	15.72%	17.72%	27.11%	17.43%	27.08%	17.55%	27.26%
CNN-LSTM	8.79%	12.39%	6.88%	9.66%	10.91%	15.33%	15.62%	23.19%	15.51%	22.63%	15.66%	22.70%
RNN-LSTM	8.98%	13.00%	7.21%	9.72%	11.68%	15.25%	16.66%	22.12%	16.13%	22.26%	15.93%	22.40%
XGB	8.81%	12.62%	7.66%	11.12%	11.90%	16.35%	11.16%	15.33%	10.91%	15.03%	14.77%	19.33%
TFT	7.12%	10.59%	4.59%	6.75%	9.83%	14.64%	9.28%	13.16%	7.35%	10.83%	13.99%	20.34%

LSTM, TPE-MSTL- XGB and TPE-MSTL-TFT.

Table 2 shows the results of the TPE-VMD-TFT and other individual models based on the proposed framework for the 24-h and 48-h ahead wind power forecasts. The lowest values are derived from TPE-VMD-TFT, and the TFT model works best in the different decomposition algorithms. This means the TPE-VMD-TFT method outperforms the TPE-EEMD-TFT and TPE-MSTL-TFT models on wind power data from all four turbines. Regarding wind turbine 1 prediction, the TPE-VMD-TFT model showed a 32.17% and 60.11% decrease in nMAE and a 35.07% and 56.96% decrease in nRMSE compared to the TPE-EEMD-TFT and TPE-MSTL-TFT models, when predicting 24-h ahead. In predicting 48-h ahead, the predicted wind power from the TPE-VMD-TFT model decreased by 18.10% and 44.72% and the value of nRMSE decreased by 15.21% and 42.43% compared to the TPE-EEMD-TFT and TPE-MSTL-TFT models. The above analysis illustrates that there are differences in the predictive effectiveness of the TFT model combined with the three models generated by the proposed framework, with the TPE-VMD-TFT approach having a lower prediction error.

For every individual model, the decomposition methods impact the proposed framework differently. The VMD decomposition algorithm performed better than EEMD and MSTL in predicting the 24-h ahead wind power generation results. The value of nMAE for the TPE-VMD-CNN-LSTM model on the wind turbine 1 data was 6.23%, a decrease of 27.56% and 44.03% compared to the TPE-EEMD- ANN and TPE-MSTL-ANN models. The value of nRMSE was 9.22%, a decrease of 24.98% and 42.77%. Most of the VMD decomposition algorithms performed better than EEMD and MSTL in

predicting 48-h ahead wind power, but there were discrepancies in the predictions of some of the models. For example, the TPE-VMD-LSTM model performs worse than the TPE-EEMD-LSTM model regarding nMAE and nRMSE values on the Wind Turbine 1 and 2 data. So it's hard to determine an optimal decomposition method for a dataset. Thus, our proposed algorithm can automatically find the most suitable parameters on other datasets and has a higher expectation of achieving high performance than other methods that fix the decomposition algorithm and model.

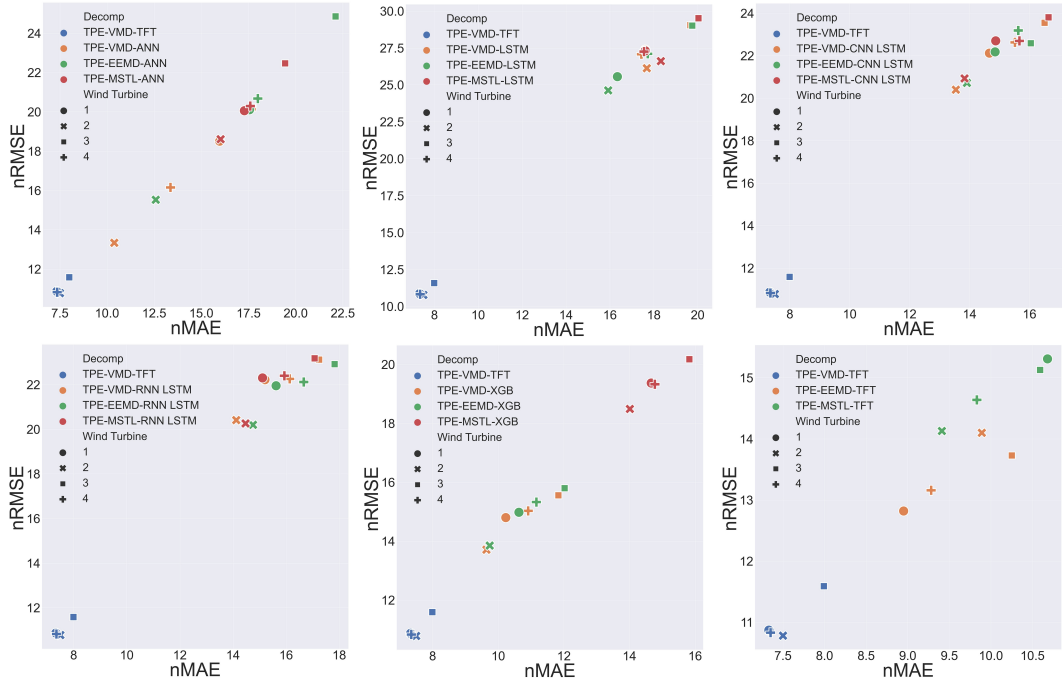


Figure 11. The scatter plot of the model's 24-h ahead forecast results.

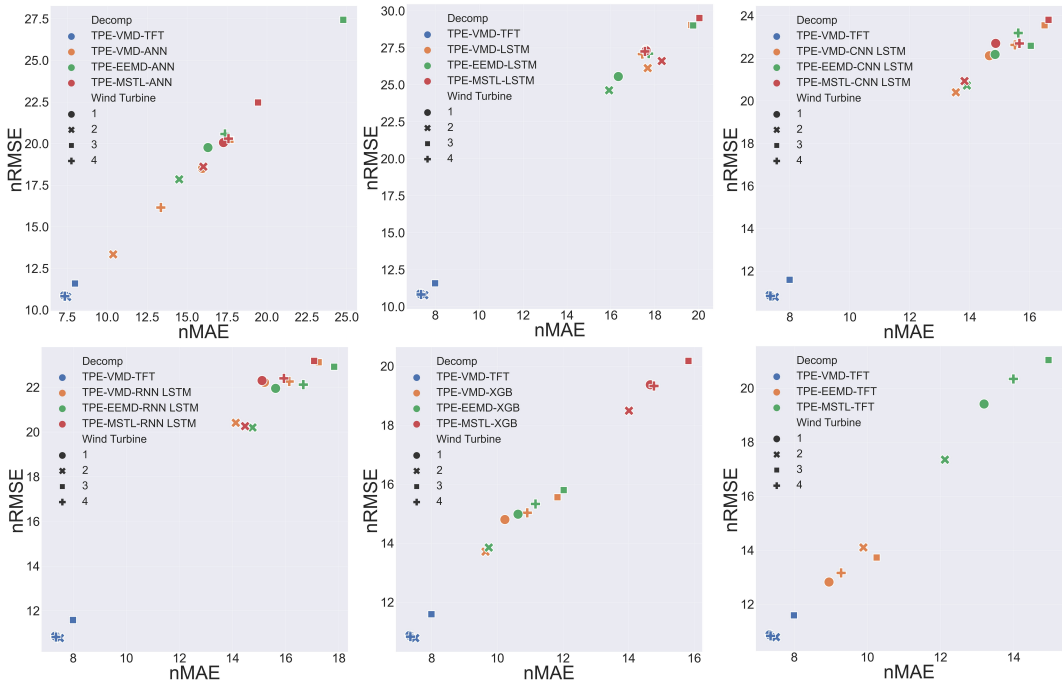


Figure 12. The scatter plot of the model's 48-h ahead forecast results.

From Table 2 and the above analysis, we find that TPE-VMD-TFT is the best of the adopted models. However, a direct discussion may not be intuitive due to the large variety of models and decomposition algorithms. Therefore, we individually compare TPE-VMD-TFT with each class of models, e.g., TPE-VMD-TFT and TPE-VMD-ANN, TPE-EEMD-ANN and TPE-MSTL-ANN. Scatter plots comparing the 24h and 48h results are shown in Figures 11 and 12. The horizon axis represents the model's nMAE value and the vertical axis represents the nRMSE value of the model. To simplify the description, the model formed by combining the proposed framework under an arbitrary decomposition algorithm is denoted as TPE-Decomp-Model. Such as TPE-Decomp-TFT denotes TPE-VMD-TFT, TPE-EEMD-TFT and TPE-MSTL-TFT.

As can be seen, the blue points representing TPE-VMD-TFT are distributed near the origin of the scatter plot on all four wind turbine data, indicating that it predicts better than the other models formed by combining the proposed framework. This suggests that the TPE-VMD-TFT method has better prediction results on the more volatile wind power data. For the scatter plots of TPE-Decomp-LSTM, TPE-Decomp-RNN-LSTM and TPE-Decomp-CNN-LSTM, the distances between their points are similar under different decomposition algorithms, so we speculate that these models are not significantly affected by different decomposition algorithms. Furthermore, the points of them and TPE-VMD-TFT are distributed in the lower left and upper right corners, indicating a large gap between TPE-Decomp-LSTM, TPE-Decomp-RNN-LSTM, TPE-Decomp-CNN-LSTM and TPE-VMD-TFT. For TPE-Decomp-ANN, TPE-Decomp-XGB and TPE-Decomp-TFT, their point distributions are more dispersed along the diagonal and the general characteristics can be seen: VMD is better than EEMD, and EEMD is better than MSTL. Therefore, decomposition algorithms have a major influence on the models, and the VMD perform best in most models.

Classification analysis based on TPE-VMD-TFT

In subsection 4.4.1, we compare the proposed TPE-VMD-TFT method with common models for wind power forecasting and find that TPE-VMD-TFT has significant advantages over the other models. Next, we applied TPE-DTBM to the other models and obtained 17 models. The results show that the proposed TPE-VMD-TFT method also outperforms these models. To further analyze and verify the validity of the TPE-VMD-TFT method, the forecasts were grouped according to month, season and year.

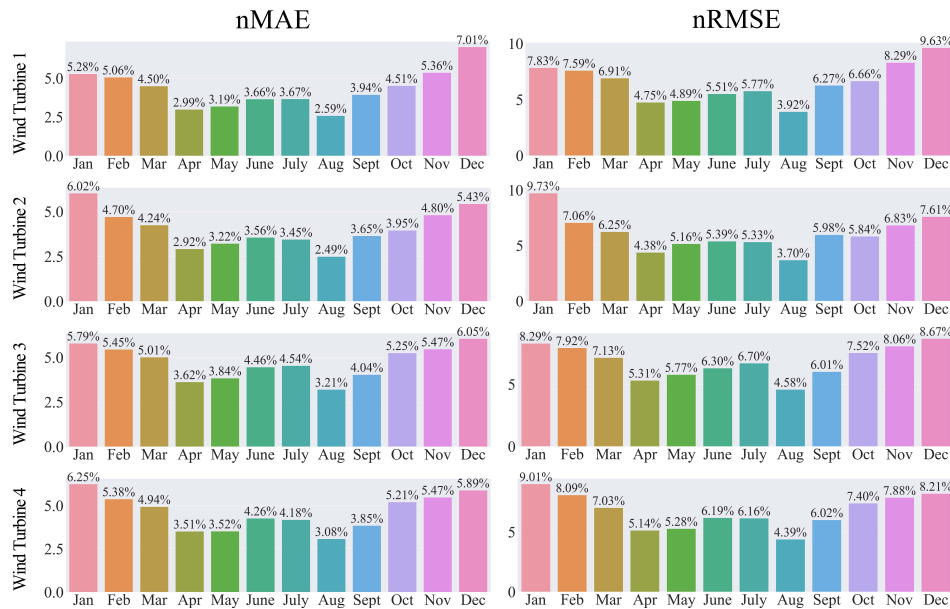


Figure 13. Monthly results of 24-h ahead forecasting based on TPE-VMD-TFT method (nMAE).

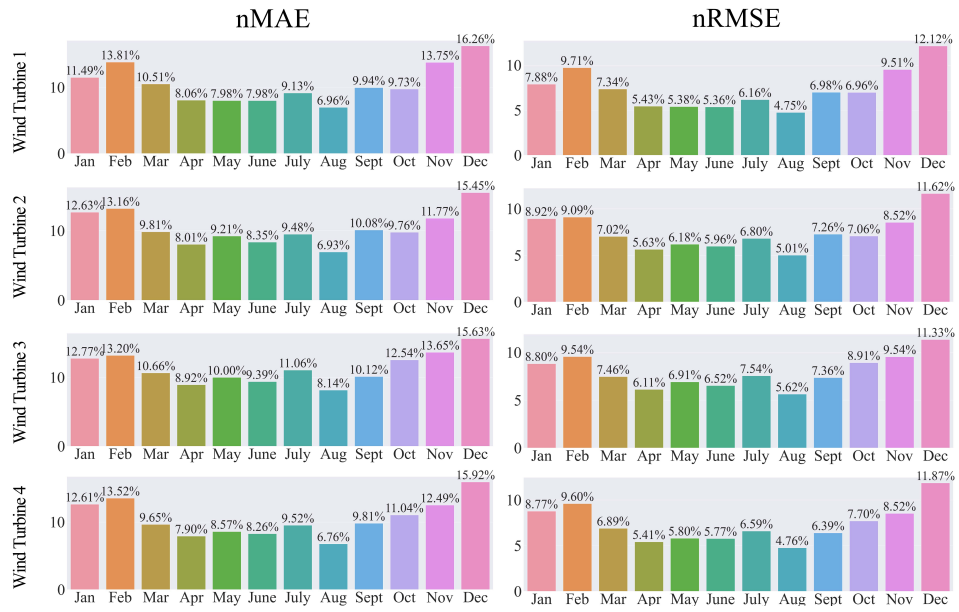


Figure 14. Monthly results of 48-h ahead forecasting based on TPE-VMD-TFT method (nMAE).

Figures 13 and 14 show the results of the TPE-VMD-TFT method for 24-h and 48-h ahead wind power forecasting by month. The horizon axis represents the months from January to December and the vertical axis represents the forecast error. From figure 13 and 14, the nMAE values for the four wind turbines range from 2% to 8% throughout the year in the predicted 24-h ahead wind power results, except for wind turbine 1, which has an nMAE value of 7.01% for December and less than 7% for all other months. Forecast errors were relatively low for April-September and relatively high for January-March and October-December. The four wind turbines had error values of 2.59%, 2.49%, 3.21% and 3.08% in August, lower than the other months of the year. In the predicted 48-h ahead wind power generation, the nMAE values for the four wind turbines ranged from 4% to 13% throughout the year. Forecast errors for December are relatively high, with nMAE values above 11%. The forecast errors for March-September are relatively low, with nMAE values all below 8%.

Figures 15 show the results of the TPE-VMD-TFT method for 24-h ahead and 48-h ahead wind power forecasting by season. The horizon axis represents the four seasons, and the vertical axis represents the prediction error. Regarding the geographical location of the wind farm, the months of March, April and May are classified as spring. June, July and August are classified as summer. September, October and November are classified as autumn. December, January and February are classified as winter. As can be seen from the graph, the prediction error values for all four wind turbines are relatively low in all seasons when predicting 24-h ahead, with nMAE values ranging from 3% to 6%. The lowest nMAE values all occurred during the summer months, at 3.3%, 3.16%, 4.06% and 3.84%. The highest nMAE values all occurred in winter, at 5.81%, 5.41%, 5.78% and 5.85%. In predicting 48-h ahead, the nMAE values for the four wind turbines ranged from 5% to 11% in all seasons, with relatively similar prediction errors in spring, summer and autumn and relatively high prediction errors in winter.

Figures 16 show the results of the TPE-VMD-TFT method for 24-h ahead and 48-h ahead wind power forecasting by year. The horizon axis represents the different years, and the vertical axis represents the forecast error. From figures 16, in predicting the results for 24-h ahead wind power, all four wind turbines have lower prediction errors in 2017 than in 2018. Wind turbine 2 has the most significant prediction difference at 3.99% and 6.49%. The forecast errors for 2017 and 2018 are relatively similar when forecasting 48-h ahead. Wind turbine 4 has almost the same prediction error, while wind turbine 1 has a more significant difference in prediction error of 7.26% and 9.63%.

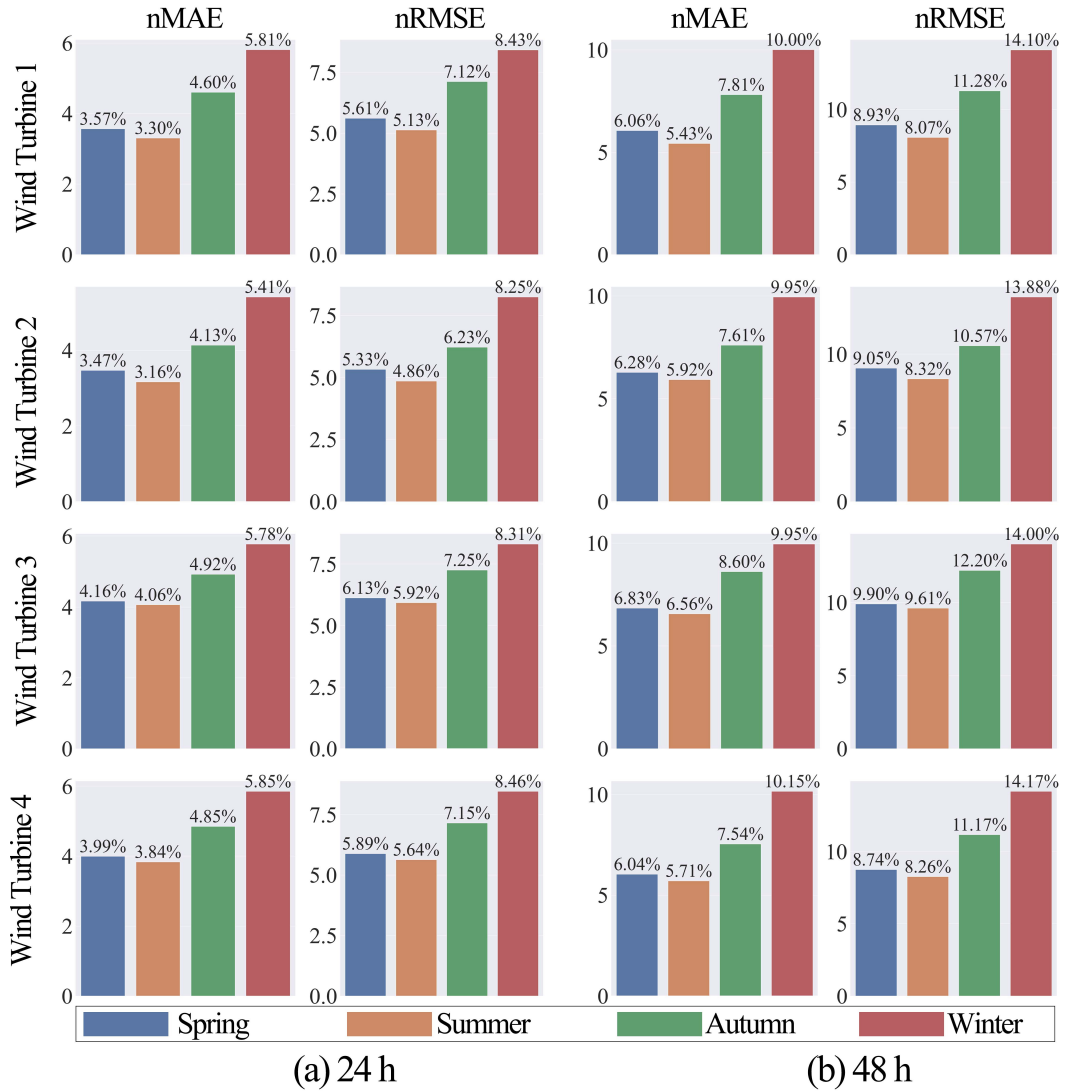


Figure 15. Seasonal results of 24-h ahead forecasting based on TPE-VMD-TFT method (nMAE).

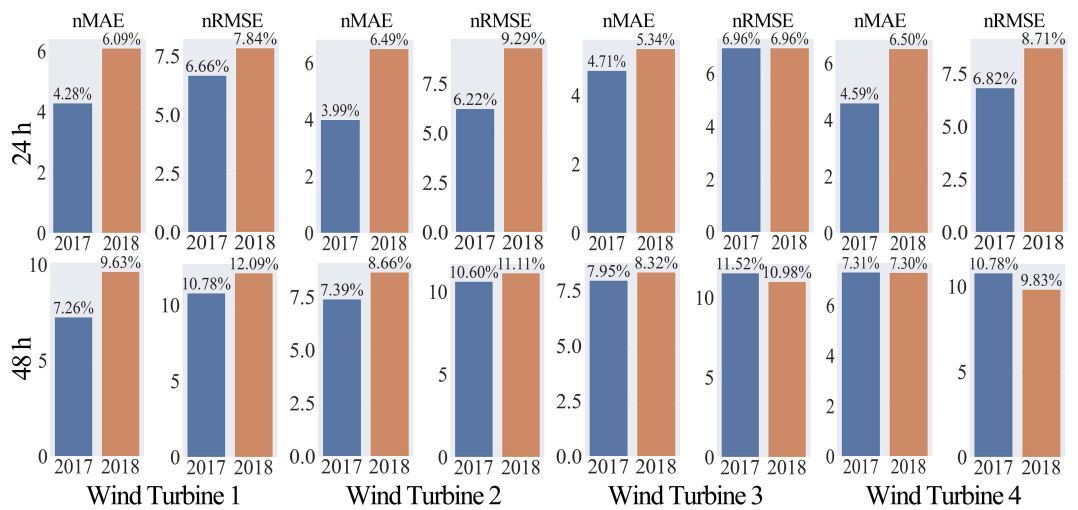


Figure 16. Annual results of 24-h ahead forecasting based on TPE-VMD-TFT method (nMAE).

From the above analysis, it can be seen that the prediction accuracy of the TPE-VMD-TFT method is relatively high in different months, seasons and years, indicating that the TPE-DTBM algorithm proposed in this paper is effective in improving the prediction performance of the TFT model.

Model stability analysis

Figure 17 are box plots of prediction errors for all wind power forecasting models. The horizon axis indicates the models involved, and the vertical axis indicates the distribution of prediction errors for the models. As the test set contains 8832 time points, even with outliers of 2%-10%, there will be at least 170 outliers per method, making it difficult to plot outliers clearly. Therefore, we still use Q1, Q2 and Q3 as the lower boundaries of the box, the median and the upper boundaries of the box in the box plot, but use the minimum and maximum values of the data as the lower and upper boundaries of the box plot. The blue boxes in the figure indicate the error distribution of individual models, the yellow boxes indicate models based on the TPE-MSTL algorithm, the green boxes indicate models based on the TPE-EEMD algorithm, and the red boxes indicate models based on the TPE-VMD algorithm. As can be seen from the graph, the median of the blue boxes is mostly higher, and the boxes are longer. This indicates that the individual models are less effective in predicting as well as being unstable. The red boxes had mostly lower median values and shorter boxes than the other colored boxes. This indicates that the model based on the TPE-VMD algorithm has better predictive performance and is more stable than the models based on the TPE-EEMD and TPE-MSTL algorithms. The TPE-VMD-TFT method has the lowest median number of boxes and the shortest boxes, indicating that this method has the most superior performance compared to the other models.

To visualize the performance of the TPE-VMD-TFT model proposed in this paper on wind power data, Figures 18 show the results of the TPE-VMD-TFT model for 24-h ahead and 48-h ahead wind power predictions. The black and red lines in the graph indicate the actual and predicted values of wind power. It can be seen from the graph that the two lines overlap more when predicting 24-h ahead, which indicates that the predicted values of wind power are closer to the actual values. Although the prediction performance of the TPE-VMD-TFT model is reduced when predicting 48-h ahead, it is reasonable. This is because predicting wind power 48-h ahead is more complex than predicting 24-h ahead, with greater instability and uncertainty in the data. In summary, for the more volatile wind power data, the TPE-VMD-TFT model's prediction curves are closer to the original wind power series, yielding higher accuracy than individual models. Decomposing the wind power series through the TPE-VMD framework to reduce the influence of noise on the prediction results can effectively extract features for the TFT model and improve the model's prediction performance.

5 Conclusion

Accurate wind power forecasting plays an essential role in the power systems scheduling and planning. However, wind power forecasting is challenging because of its high uncertainty, discontinuity and violent fluctuations. In this paper, we propose a novel medium-term forecasting framework based on TPE and decomposition algorithms that define the TPE-VMD-TFT method to predict wind power from wind turbine. Much of the literature is based on the empirical selection of the hyper-parameters of the decomposition algorithm, which can lead to predictions that are not optimal. To alleviate these problems, we propose a TPE-DTBM algorithm. The TPE-DTBM algorithm is not only the critical method of the TPE-VMD-TFT approach, but also be generalized to other common decomposition algorithms and models for wind power forecasting. We conducted experiments using the Engie wind dataset from the electricity company in France and used nMAE and nRMSE to evaluate the performance of the proposed method.

The values of nMAE for our proposed method for 24-h ahead wind power prediction were 4.26%, 4.02%, 4.63% and 4.59% for the four wind turbines and 6.59%, 6.21%, 6.78% and 6.75% for the

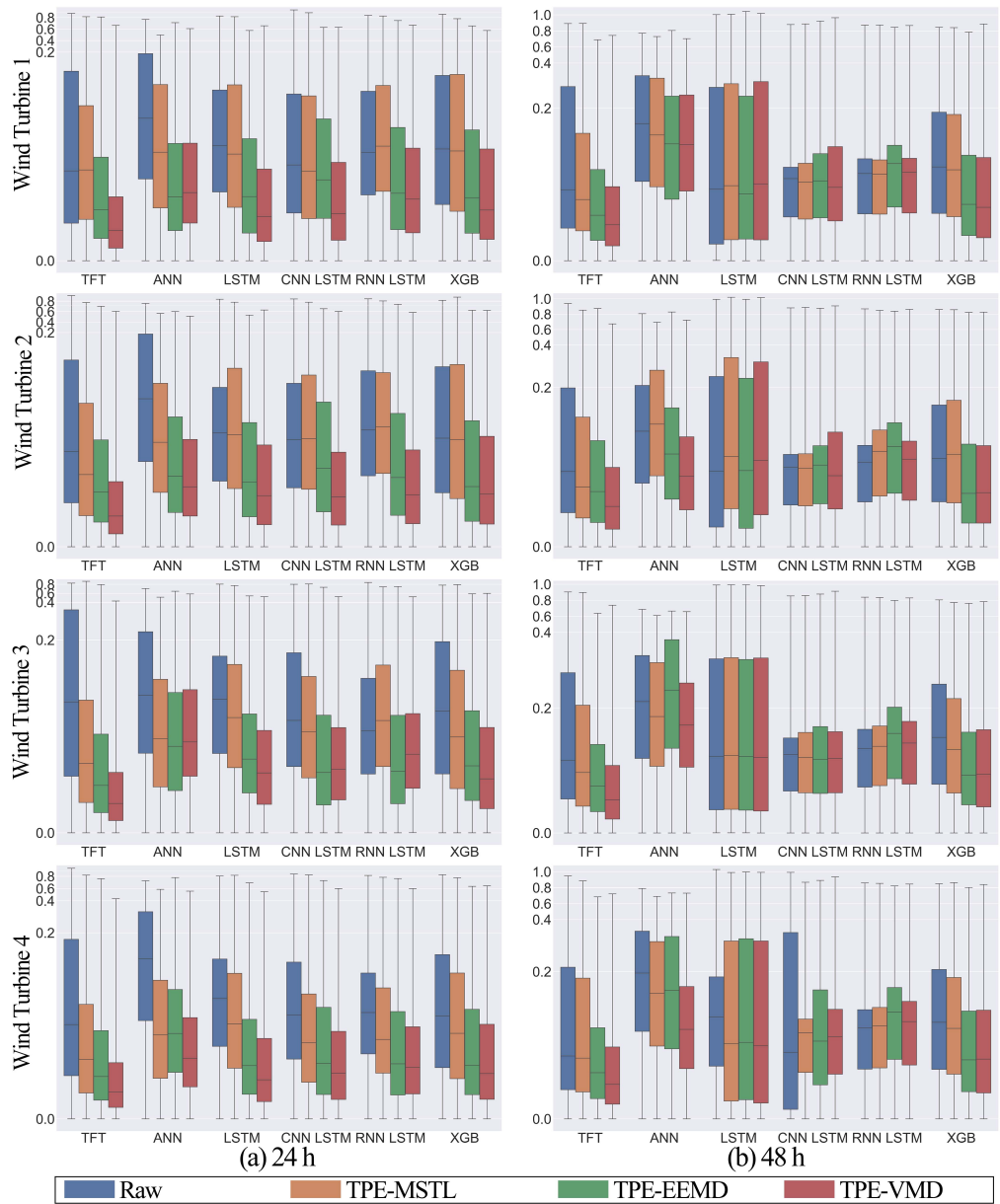


Figure 17. Box plot of the error of the model for 24-h ahead prediction.

nRMSE respectively. At the predicted 48-h ahead, the values for nMAE were 7.33%, 7.5%, 7.99% and 7.35%, and the values for nRMSE were 10.87%, 10.78%, 11.59% and 10.83%. Compared to other individual time series prediction models (e.g. ANN, LSTM, CNN-LSTM, RNN-LSTM and XGB), the nMAE values were reduced by more than 50% and the nRMSE values were reduced by more than 40%. Compared with wind power generation forecasting methods that obtain data features through other decomposition algorithms, the forecasting effect of the proposed method is also better than these models. The TPE-VMD-TFT method uses the TPE-DTBM algorithm to optimize the parameters of the VMD to decompose the wind power series, which can effectively extract the characteristics of the wind power and reduce the noise of the historical data, significantly improving the prediction accuracy.

To further analyze and verify the validity of the TPE-VMD-TFT method, the forecasts were grouped according to month, season and year. The experiments prove that the proposed method

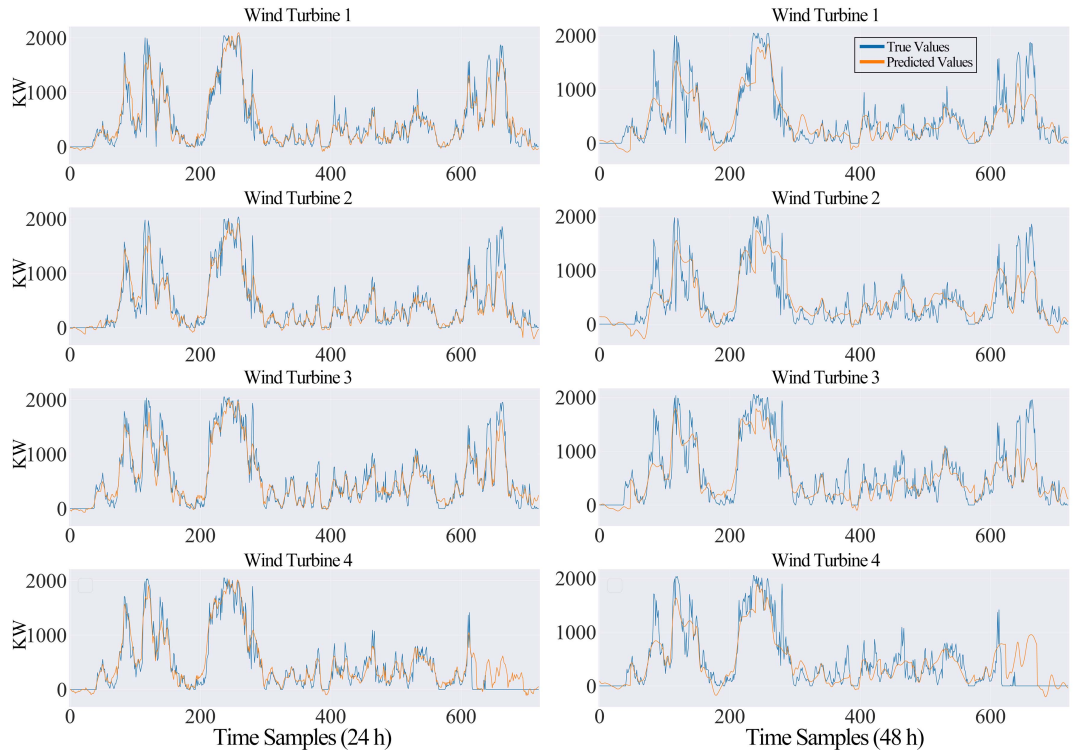


Figure 18. 24-h ahead prediction results of the TPE-VMD-TFT model.

has high prediction accuracy in different months, seasons and years, indicating that the TPE-DTBM algorithm proposed in this paper effectively improves the prediction performance of the TFT model. A box plot of the wind power forecasting model's prediction errors demonstrates the proposed method's higher stability compared to other comparative models.

In the wind power forecasting problem, the novel medium-term forecasting framework proposed in this paper and the defined TPE-VMD-TFT method have superior forecasting performance and generalization capability. However, there are still many issues that need to be investigated. For example, data sets from different geographical locations are not considered. This is because meteorological data also differ from region to region, resulting in differences in prediction accuracy. In addition, the proposed framework for wind power prediction can be tried to be extended to other energy prediction areas, such as photovoltaic power and wind speed prediction, which is also the direction of our future efforts.

Acknowledgments. TBD

Data Availability Statement. TBD

References

- [1] *UN Climate Action*. Apr. 2023. URL: <https://www.un.org/en/climatechange/science/causes-effects-climate-change>.
- [2] Yun Wang *et al.* “Approaches to wind power curve modeling: A review and discussion”. In: *Renewable and Sustainable Energy Reviews* 116 (2019), p. 109422.
- [3] *GWEC 2022*. Apr. 2022. URL: <https://gwec.net/global-wind-report-2022/>.
- [4] Jaesung Jung and Robert P Broadwater. “Current status and future advances for wind speed and power forecasting”. In: *Renewable and Sustainable Energy Reviews* 31 (2014), pp. 762–777.
- [5] Wen-Yeau Chang *et al.* “A literature review of wind forecasting methods”. In: *Journal of Power and Energy Engineering* 2.04 (2014), p. 161.
- [6] Gamal Aburiyana and Mohamed E El-Hawary. “An overview of forecasting techniques for load, wind and solar powers”. In: *2017 IEEE Electrical Power and Energy Conference (EPEC)*. IEEE. 2017, pp. 1–7.
- [7] A Shobana Devi *et al.* “Hourly day-ahead wind power forecasting with the EEMD-CSO-LSTM-EFG deep learning technique”. In: *Soft Computing* 24.16 (2020), pp. 12391–12411.
- [8] Shahram Hanifi *et al.* “A critical review of wind power forecasting methods—past, present and future”. In: *Energies* 13.15 (2020), p. 3764.
- [9] Saurabh S Soman *et al.* “A review of wind power and wind speed forecasting methods with different time horizons”. In: *North American power symposium 2010*. IEEE. 2010, pp. 1–8.
- [10] Yun Wang *et al.* “A review of wind speed and wind power forecasting with deep neural networks”. In: *Applied Energy* 304 (2021), p. 117766.
- [11] Jing Yan and Tinghui Ouyang. “Advanced wind power prediction based on data-driven error correction”. In: *Energy conversion and management* 180 (2019), pp. 302–311.
- [12] Thomas Ackermann and Lennart Söder. “Wind energy technology and current status: a review”. In: *Renewable and sustainable energy reviews* 4.4 (2000), pp. 315–374.
- [13] Lazar Lazić, Goran Pejanović, and Momčilo Živković. “Wind forecasts for wind power generation using the Eta model”. In: *Renewable Energy* 35.6 (2010), pp. 1236–1243.
- [14] Ulrich Focken, Matthias Lange, and Hans-Peter Waldl. “Previento—a wind power prediction system with an innovative upscaling algorithm”. In: *Proceedings of the European Wind Energy Conference, Copenhagen, Denmark*. Vol. 276. 2001.
- [15] Ma Lei *et al.* “A review on the forecasting of wind speed and generated power”. In: *Renewable and sustainable energy reviews* 13.4 (2009), pp. 915–920.
- [16] Eddie Yatiyana, Sumedha Rajakaruna, and Arindam Ghosh. “Wind speed and direction forecasting for wind power generation using ARIMA model”. In: *2017 Australasian Universities Power Engineering Conference (AUPEC)*. IEEE. 2017, pp. 1–6.
- [17] Umut Firat *et al.* “Wind speed forecasting based on second order blind identification and autoregressive model”. In: *2010 Ninth International Conference on Machine Learning and Applications*. IEEE. 2010, pp. 686–691.
- [18] Boudy Bilal *et al.* “Wind turbine power output prediction model design based on artificial neural networks and climatic spatiotemporal data”. In: *2018 IEEE International Conference on Industrial Technology (ICIT)*. IEEE. 2018, pp. 1085–1092.
- [19] Lei Xu and Jiandong Mao. “Short-term wind power forecasting based on Elman neural network with particle swarm optimization”. In: *2016 Chinese Control and Decision Conference (CCDC)*. IEEE. 2016, pp. 2678–2681.

- [20] M Nandana Jyothi and PV Ramana Rao. "Very-short term wind power forecasting through adaptive wavelet neural network". In: *2016 Biennial International Conference on Power and Energy Systems: Towards Sustainable Energy (PESTSE)*. IEEE. 2016, pp. 1–6.
- [21] G Peter Zhang and Min Qi. "Neural network forecasting for seasonal and trend time series". In: *European journal of operational research* 160.2 (2005), pp. 501–514.
- [22] Jing Shi, Jinmei Guo, and Songtao Zheng. "Evaluation of hybrid forecasting approaches for wind speed and power generation time series". In: *Renewable and Sustainable Energy Reviews* 16.5 (2012), pp. 3471–3480.
- [23] Yurong Wang, Dongchuan Wang, and Yi Tang. "Clustered hybrid wind power prediction model based on ARMA, PSO-SVM, and clustering methods". In: *IEEE Access* 8 (2020), pp. 17071–17079.
- [24] Rashmi P Shetty, APSP Sathyabhama, A Adarsh Rai, et al. "Optimized radial basis function neural network model for wind power prediction". In: *2016 second international conference on cognitive computing and information processing (CCIP)*. IEEE. 2016, pp. 1–6.
- [25] Aneela Zameer et al. "Intelligent and robust prediction of short term wind power using genetic programming based ensemble of neural networks". In: *Energy conversion and management* 134 (2017), pp. 361–372.
- [26] Jinqiang Liu, Xiaoru Wang, and Yun Lu. "A novel hybrid methodology for short-term wind power forecasting based on adaptive neuro-fuzzy inference system". In: *Renewable energy* 103 (2017), pp. 620–629.
- [27] Yixiao Yu et al. "Probabilistic prediction of regional wind power based on spatiotemporal quantile regression". In: *2019 IEEE Industry Applications Society Annual Meeting*. IEEE. 2019, pp. 1–16.
- [28] Zhewen Niu et al. "Wind power forecasting using attention-based gated recurrent unit network". In: *Energy* 196 (2020), p. 117081.
- [29] Anbo Meng et al. "A hybrid deep learning architecture for wind power prediction based on bi-attention mechanism and crisscross optimization". In: *Energy* 238 (2022), p. 121795.
- [30] Vijaya Krishna Rayi et al. "Adaptive VMD based optimized deep learning mixed kernel ELM autoencoder for single and multistep wind power forecasting". In: *Energy* 244 (2022), p. 122585.
- [31] Jiandong Duan et al. "A novel hybrid model based on nonlinear weighted combination for short-term wind power forecasting". In: *International Journal of Electrical Power & Energy Systems* 134 (2022), p. 107452.
- [32] Sepp Hochreiter and Jürgen Schmidhuber. "Long short-term memory". In: *Neural computation* 9.8 (1997), pp. 1735–1780.
- [33] Tianqi Chen and Carlos Guestrin. "Xgboost: A scalable tree boosting system". In: *Proceedings of the 22nd acm sigkdd international conference on knowledge discovery and data mining*. 2016, pp. 785–794.
- [34] Bryan Lim et al. "Temporal fusion transformers for interpretable multi-horizon time series forecasting". In: *International Journal of Forecasting* 37.4 (2021), pp. 1748–1764.
- [35] Djork-Arné Clevert, Thomas Unterthiner, and Sepp Hochreiter. "Fast and accurate deep network learning by exponential linear units (elus)". In: *arXiv preprint arXiv:1511.07289* (2015).
- [36] Norden E Huang et al. "The empirical mode decomposition and the Hilbert spectrum for nonlinear and non-stationary time series analysis". In: *Proceedings of the Royal Society of London. Series A: mathematical, physical and engineering sciences* 454.1971 (1998), pp. 903–995.
- [37] Zhaohua Wu and Norden E Huang. "Ensemble empirical mode decomposition: a noise-assisted data analysis method". In: *Advances in adaptive data analysis* 1.01 (2009), pp. 1–41.
- [38] Zengshun Chen et al. "An Improved Method Based on EEMD-LSTM to Predict Missing Measured Data of Structural Sensors". In: *Applied Sciences* 12.18 (2022), p. 9027.
- [39] Konstantin Dragomiretskiy and Dominique Zosso. "Variational mode decomposition". In: *IEEE transactions on signal processing* 62.3 (2013), pp. 531–544.

- [40] Robert B Cleveland *et al.* “STL: A seasonal-trend decomposition”. In: *J. Off. Stat* 6.1 (1990), pp. 3–73.
- [41] Kasun Bandara, Rob J Hyndman, and Christoph Bergmeir. “MSTL: a seasonal-trend decomposition algorithm for time series with multiple seasonal patterns”. In: *arXiv preprint arXiv:2107.13462* (2021).
- [42] Guoqing An *et al.* “Ultra-short-term wind power prediction based on PVMD-ESMA-DELM”. In: *Energy Reports* 8 (2022), pp. 8574–8588.
- [43] Min Yu *et al.* “A novel framework for ultra-short-term interval wind power prediction based on RF-WOA-VMD and BiGRU optimized by the attention mechanism”. In: *Energy* (2023), p. 126738.
- [44] Hua Li *et al.* “An optimized VMD method and its applications in bearing fault diagnosis”. In: *Measurement* 166 (2020), p. 108185.
- [45] Takuya Akiba *et al.* “Optuna: A next-generation hyperparameter optimization framework”. In: *Proceedings of the 25th ACM SIGKDD international conference on knowledge discovery & data mining*. 2019, pp. 2623–2631.
- [46] *Engie Data Set*. Apr. 2023. URL: <https://opendata-renewables.engie.com/explore/dataset/6eeb7f50-97f7-4ab2-8d36-c6d9f9491d84/information>.